Netrin-1 blockade inhibits tumor associated Myeloid-derived suppressor cells, cancer stemness and alleviates resistance to chemotherapy and immune checkpoint inhibitor

Benjamin Ducarouge, Anna-Rita Redavid, Camille Victoor, Ruxanda Chira, Aurélien Fonseca, Maëva Hervieu, Roméo Bergé, Justine Lengrand, Pauline Vieugué, David Neves, et al.

Netrin-1 blockade inhibits tumor associated Myeloid-derived suppressor cells, cancer stemness and alleviates resistance to chemotherapy and immune checkpoint inhibitor

Benjamin Ducarouge[1,2*], Anna-Rita Redavid[1*], Camille Victoor[1,2], Ruxanda Chira[1,2] Aurélien Fonseca[3], Maëva Hervieu[1], Roméo Bergé[1,2], Justine Lengrand[1,2], Pauline Vieugué[1], David Neves[2], Isabelle Goddard[1], Mathieu Richaud[1], Pierre-Alexandre Laval[1], Nicolas Rama[1], David Goldschneider[2], Andrea Paradisi[1], Nicolas Gourdin[4], Sylvie Chabaud[5], Isabelle Treilleux[5], Nicolas Gadot[6], Isabelle Ray-Coquard[6], Stéphane Depil[2], Didier Decaudin[7], Fariba Némati[7], Elisabetta Marangoni[7], Eliane Mery-Lamarche[8], Catherine Génestie[9], Séverine Tabone-Eglinger[6], Mojgan Devouassoux-Shisheboran[10], Kathryn J Moore[11], Benjamin Gibert[1$£], Patrick Mehlen[1,2$£] and Agnes Bernet[1,2£]

[1]Apoptosis, Cancer and Development Laboratory- Equipe labellisée 'La Ligue', Labex DEVweCAN, Institut Convergence PLAsCAN, Centre de Cancérologie de Lyon, INSERM U1052-CNRS UMR5286, Université de Lyon, Centre Léon Bérard, 69008 Lyon, France. [2]Netris Pharma, Centre Léon Bérard, 69008 Lyon, France. [3]Research Pathology Department, Centre Léon Bérard, Lyon, France. [4]Targeting of the tumor and its immune environnement, Centre de Cancérologie de Lyon, INSERM U1052-CNRS UMR5286, Université de Lyon, Centre Léon Bérard, 69008 Lyon, France. [5]UBET, Centre Léon Bérard, Lyon, France. [6]Pathology Department, Centre Léon Bérard, Lyon, France. [7]Laboratory of Preclinical Investigations, Translational Research Department, Institut Curie, Université Paris-Sciences-et-Lettres, 75005 Paris, France.[8]Department of Pathology, IUCT Oncopole, Toulouse, France.[9]Department of Pathology, Gustave Roussy, Villejuif, France.[10]Hospices Civils de Lyon, Department of Pathology, 69002 Lyon, France [11]Department of Medicine, Leon H. Charney Division of Cardiology, New York University School of Medicine, New York, New York, USA.

[$]Corresponding authors: P. Mehlen; e-mail: patrick.mehlen@lyon.unicancer.fr , A. Bernet; e-mail: agnes.bernet@lyon.unicancer.fr and B. Gibert; e-mail: benjamin.gibert@lyon.unicancer.fr

[£]Co-senior authors

Abstract:

Drug resistance and cancer relapse represent significant therapeutic challenges after chemotherapy or immunotherapy, and a major limiting factor for long-term cancer survival. Netrin-1 was initially identified as a neuronal navigation cue but has more recently emerged as an interesting target for cancer therapy, which is currently clinically investigated. We show here that netrin-1 is an independent prognostic marker for clinical progression of breast and ovary cancers. Cancer stem cells (CSCs)/Tumor initiating cells (TICs) are hypothesized to be involved in clinical progression, tumor relapse and resistance. We found a significant correlation between netrin-1 expression and cancer stem cell (CSC) markers levels. We also show in different mice models of resistance to chemotherapies that netrin-1 interference using a therapeutic netrin-1 blocking antibody alleviate resistance to chemotherapy and triggers an efficient delay in tumor relapse and that this effect is associated with CSCs loss. We also demonstrate that netrin-1 interference limits tumor resistance to immune checkpoint inhibitor and provide evidence linking this enhanced anti-tumor efficacy to the blockage of recruitment of a subtype of myeloid-derived suppressor cells (MDSCs) called PMN-MDSCs. We have functionally demonstrated that these immune cells promote CSCs and, consequently, resistance to anti-cancer treatments. Together, these data support the view of both a direct and indirect contribution of netrin-1 to cancer stemness and we propose that this may lead to therapeutic opportunities by combining conventional chemotherapies and immunotherapies with netrin-1 interfering drugs.

Introduction:

Netrin-1 is a multifunctional, secreted, laminin-related glycoprotein that plays key roles in neuronal navigation, angiogenesis, and cell survival[1–3]. Netrin-1 is also implicated in numerous pathologies including type 2 diabetes, cardiovascular disease, and cancer[4–9]. Its activity has been shown to principally occur through the regulation of the signaling pathways transduced by its main receptors, Deleted in Colorectal Carcinoma (DCC) and UNC5-Homolog (UNC5H- *i.e.*, UNC5A, UNC5B, UNC5C, UNC5D)[10,11]. Notably, netrin-1 has been shown to be up-regulated in many tumor types, and this up-regulation has been proposed to act as a selective mechanism that blocks apoptosis induced by the dependence receptors DCC and UNC5B[4,12].

Efforts to develop drugs that inhibit the interaction of netrin-1 with its receptors have therefore been initiated. Several pre-clinical proof-of-concept studies have highlighted that candidate drugs interfering with netrin-1-receptor interactions markedly inhibit tumor growth and metastasis[13–16]. NP137, a netrin-1 targeted monoclonal antibody strongly accumulate within tumors and was recently evaluated in a phase I clinical trial among patients with advanced solid cancers[17,18]. Interim results included both excellent safety profiles and encouraging signs of clinical activity, particularly for gynecological indications[19]. Benefits were seen in patients despite highly advanced disease resistant to standard of care, including chemotherapies and immune checkpoint inhibitors[20,21].

A common view is that resistance to these anti-proliferative drugs is intrinsically linked to the presence of Cancer Stem Cells (CSCs) or Tumor-Initiating Cells (TICs) within the tumors. The notion is that CSCs and TICs rely on the existence of a distinct subset of tumor cells that possesses the capacity to sustain tumor growth[22]. CSCs/TICs are thought to express specific markers at the cell surface and are identified functionally based on their ability to propagate tumors when serially transplanted into recipient mice[23]. Whether CSCs are a distinct subset of cancer cells, or whether they represent a functional state of some cancer cells, remains a matter of debate. To date, the general consensus is that CSCs are key to clinical progression due to their ability to self-renew and resist chemotherapies or more recently to immune checkpoint inhibitors[24–28], thereby facilitating tumor relapse[29].

In the present study, we thus investigated netrin-1 implication in breast and ovary and its putative link with cancer stemness and resistance to

chemotherapy/immunotherapy. We show that netrin-1 expressed by cancer stem cells promotes resistance to anticancer drugs. We also associate netrin-1 expression with clinical progression and demonstrate that in various animal models, netrin-1 interference selectively impacts CSCs/TICs, thus potentiating sensitivity to chemotherapy and anti-CTLA-4 monoclonal Antibody (mAb) immunotherapy. Finally, we describe the integration of netrin-1 within the tumoral microenvironment and show that the anti-netrin-1 inhibits tumor recruitment of a subtype of myeloid-derived suppressor cells (MDSCs) called PMN-MDSCs. We provide functional evidence that these immune cells promote the CSC phenotype, and consequent resistance to anti-cancer treatments.

Results:

Netrin-1 expression is associated with clinical progression and cancer stemness in ovary and breast tumors.

Previous studies described high-level netrin-1 expression in a sizeable fraction of human breast and ovarian cancers[13,17,30]. Moreover, patients with metastasis at diagnosis harbored primary tumors with greater netrin-1 expression than patients who were metastasis-free[13]. To evaluate the impact of netrin-1 on prognosis, we analyzed tumor expression of netrin-1 by quantitative-RT-PCR (q-RT-PCR) across a panel of 89 breast cancer patients treated with conventional chemotherapies, correlating netrin-1 expression data with clinical data. Clinical characteristics of the patients are presented in **Supplementary Table 1**. Patients with tumors with elevated netrin-1 expression had a significantly worse prognosis than patients with tumors with low netrin-1 expression. The median survival of breast cancer patient was 9.8 years in the high netrin-1 group. By contrast, the median survival was not yet reached at 15 years in the low netrin-1 group (**Fig. 1A**). Importantly, netrin-1 expression emerged as an independent prognostic factor in multivariate analysis, together with the presence of metastasis at diagnosis (**Supp. Table 2**). To better evaluate the association between netrin-1 expression and the risk of tumor relapse or progression, we evaluated the prognostic value of netrin-1 tumor expression in the 67 patients with a localized disease, using treatment-free survival as an endpoint in this retrospective analysis. As shown in **Figure 1B**, median treatment-free survival was 9.9 years for patients with high netrin-1 tumor and was not reached for low netrin-1 group.

CSCs/TICs are hypothesized to play a major role in clinical progression and tumor recurrence[22,31,32]. As shown in **Figure 1C**, netrin-1 expression was significantly elevated in CSC marker CD44 high tumors *vs* CD44 low tumors (n=89). Similar data were obtained with other CSC markers (**Supp. Fig. 1A**). In parallel, using fresh tumoral tissues from patients, we generated mammospheres to enrich stem-like subpopulations. We observed that netrin-1 expression is lower in the overall bulk tumor as compared to the paired mammospheres (**Fig. 1D**), indicating an enrichment of netrin-1 in the subpopulation of cancer cells capable of regenerating spheres.

To analyze whether the results obtained in breast cancer could be extended to other pathologies, we have investigated by immunohistochemistry (IHC) analysis the expression of netrin-1 in ovarian carcinomas (**Supp. Fig.1B**). IHCs were performed on biological samples taken at diagnosis in a cohort of 51 patients with high-grade serous ovarian carcinomas without neoadjuvant therapy. Clinical characteristics of the patients are presented in **Supplementary Table 3.** As shown in **Figure 1E**, patients had a significantly poorer prognosis with increasing netrin-1 expression. Median survivals were respectively 9.9, 5.7 and 3.3 years in the Negative, Low and High netrin-1 groups respectively. As shown in **Figure 1F**, median treatment-free survivals were respectively 5.6, 3.1 and 1.8 years for patients with Negative, Low and High expression of netrin-1 within the tumor. Similarly, netrin-1 was elevated in patients whose tumors were resistant to platinum therapy (**Fig. 1G**) and increasing netrin-1 was concordant with the CA-125, a circulating tumor marker known to correlate with tumor relapse (**Supplementary Fig. 1C**). To determine the association of netrin-1 expression with the CD44 stem marker, we performed q-RT-PCR analysis on a cohort of 22 patients with high-grade serous ovarian carcinoma. As shown in **Figure 1H**, netrin-1 expression was significantly higher in High CD44 tumors than in Low CD44 tumors. Taken together, these expression data suggest that the level of netrin-1 is associated with relapse and progression of breast and ovarian tumors and that netrin-1 is specifically upregulated in CSCs/TICs compared to the bulk tumor.

The expression of netrin-1 in patient's tumors and its association with CSCs/TICs led us to investigate the link between netrin-1 expression and stem properties in a series of breast and ovarian cancer cell lines. With the idea that chemoresistance is associated with stemness, we first identified Hs578t and SKBR7 as partially chemo-sensitive to Adriamycin (*i.e.,* ~20% of cells are still alive after 48h of Adriamycin (**Supp. Fig. 2A**)) relative to other netrin-1 positive human cell lines screened. Interestingly, following Adriamycin treatment, the surviving Hs578t and SKBR7 cells were enriched for stem cell markers such as CD44 or CD49f, as well as netrin-1 (**Fig. 2A**; **Supp. Fig. 2B-C**). We next investigated the ability of cells to form spheres in breast and ovarian cell lines as a functional test to identify the existence of a stem cell population. BT474, Hs578t, and OV90 form spheres (**Supp. Fig. 2D**) and we observed a concordant elevation of stem cell markers and netrin-1, when compared to the parental 2D cultures (**Fig. 2B; Supp. Fig. 2E**). To avoid the potential bias of

analyzing CSCs enrichment after chemotherapy or sphere formation, we also performed an unbiased examination of netrin-1 expression in cells after sorting for stem cell markers positivity. Hs578t, SKBR7 breast cancer cells and OV90 ovary cancer cells have been sorted for respectively CD49f, ALDH or CD44 markers positivity associated with a clear increase of netrin-1 (**Fig. 2C**; **Supp. Fig. 2F-G**). This result highlights the association between netrin-1 and functional CSC markers in different tumor types.

In order to evaluate the involvement of netrin-1 in CSCs/TICs-mediated treatment resistance, we first took advantage of a patient-derived xenograft (PDX) immunocompromised mouse model in which a human triple negative breast tumor sample -*i.e.*, HBC146- is grafted. This model was shown to be sensitive to a single injection of chemotherapeutic agents, such as adriamycin and cyclophosphamide[33]. Human residual disease pathology includes a remission phase during which the tumor is virtually undetectable, followed by a relapse phase in ~80% of the mice (**Fig. 2D**). Netrin-1 expression was relatively low in the tumor bulk during the tumor growth phase but was markedly elevated during the regression phase, returning to the basal level at the time of relapse (**Fig. 2E**). Of interest, netrin-1 level appears fully correlated with the presence of CD44 marker during all these stages, indicating a strong association of netrin-1 with the stem character of the tumor cells (**Fig. 2E**). In order to link these higher expression levels of netrin-1 and CD44 with an enrichment of CSCs during the tumor regression phase more specifically, we dissected out untreated tumors or chemotherapy-treated tumors prior to complete regression and performed CD44 analysis by flow cytometry or mammospheres forming assays. $CD44^{high}$ cells were enriched during the regression phase (**Fig. 2F**). Consistent with reports of CSC resistance to chemotherapy, mammospheres formation occurred more frequently when the tumors cells used were derived immediately following chemotherapy (**Fig. 2G**). We then proceeded to the enrichment of tumor-initiating cells from the untreated tumor, either by $CD44^{high}$ sorting or by mammospheres' cultures. Netrin-1 expression was enriched in $CD44^{high}$ cells (Supp. **Fig. 2H**). Paralleling our results in human breast cancer samples, netrin-1 was less expressed in bulk tumors than in mammospheres generated from these same tumors (**Fig. 2H**). Taken together, these data support the view that in this breast cancer PDX model, netrin-1 is only weakly expressed in bulk

tumors but is more strongly expressed in a population of tumors cells resistant to the chemotherapeutic treatment that display elevated CSC markers.

Netrin-1 blockade induces cell death and delays relapse.

We and others groups have shown that netrin-1 up-regulation is a mechanism of escape from netrin-1 dependence receptor-induced apoptosis[13–16,34]. In order to investigate the potential survival role of netrin-1 in CSC, we first knocked down netrin-1 expression by siRNA in different cell lines. Silencing of netrin-1 is associated with cell death induction in Hs578t as measured by a SubG1 assay (**Fig. 2I**). Moreover, this effect is increased when Adriamycin is combined as measured by cell viability (**Fig. 2J**). Along the same line, netrin-1 silencing impairs sphere formation ability of both Hs578t and OV90 cells (**Fig. 2K**).

In order to achieve a pre-clinical and clinical development of targeting netrin-1, a specific blocking monoclonal antibody (mAb) has been developped[19,35]. When we examined the effect of this antibody (mAb) in the previously described HBC146-PDX model, we found that systemic delivery of the anti-netrin-1 mAb did not reveal any significant tumor growth-inhibiting effect (**Supp. Fig. 3A**). This was consistent with the low level of netrin-1 expressed in this tumor. However, evaluating this together with combined chemotherapy, we observed a marked decrease of tumor regrowth at the expected time of relapse observed in the chemotherapy-treated mice (**Fig. 3A**). While the relapse-free median time in chemotherapy-treated animals was 56 days, this was significantly delayed (*i.e.*, beyond the 75 days indicating the end of the experiment) in the anti-netrin1 mAb-treated group (**Fig. 3B**). Consistent with a selective effect of netrin-1 blockade on CSCs/TICs, the anti-netrin1 mAb treatment was associated with an increase of cell death associated with a decrease in the number of cells able to form spheres (**Fig. 3C**). This result was confirmed by immunohistochemical staining of CD44, where anti-netrin-1 mAb-treated tumors showed a decrease of this stemness marker in residual cancer cells (**Fig. 3D**).

To more definitively test the ability of netrin-1 blockade to impact mammary TICs in this model, we next performed serial transplant assays. HBC146 breast tumors were initially grafted in mice and treated twice weekly with either anti-netrin-1 mAb or a control IgG1. After 32 days, tumors were dissociated and regrafted into new recipient mice to evaluate tumor take in the absence of further treatment. As shown in **Figure**

3E, anti-netrin-1 treatment is associated with a significant reduced tumor take in HBC146 serial transplantation assay. Importantly, similar results were obtained in a second breast cancer PDX model (BRE-012) where anti-netrin-1 treatment similarly failed to inhibit tumor growth (**Supp. Fig. 3B)** but was associated with a dramatic suppression of tumor take in serial transplantation assay (**Fig. 3F**).

To determine whether the results could be extended to other type of tumors, we next performed a combination treatment using anti-netrin-1 with the standard of care Carboplatin/Paclitaxel chemotherapy in the ovarian OV21 PDX model. Again, anti-netrin-1 mAb had no activity as a single agent (**Supp. Fig. 3C)** but combining anti-netrin-1 mAb with chemotherapeutic treatment triggered a better significant efficacy than chemotherapy alone (**Fig.3G**). Similar effects were obtained with ovarian OV90 cells xenografts (**Supp. Fig. 3D)**. This observation was associated with inhibition of tumor take in a serial transplantation with anti-netrin-1 alone (**Supp. Fig. 3E**). This was confirmed in mice engrafted with in high-grade serous ovarian carcinoma cell lines OV90 and OVCAR3, where no inhibition of initial tumor growth was seen with anti-netrin-1 mAb (**Supp. Fig.3F-G**) but where strong inhibition of tumor take in a serial transplantation assay was observed (**Fig. 3H-I**). Because in cancer settings the netrin-1 receptor involved appears to be mainly UNC5B, we have here investigated whether the impact on CSCs was dependent on UNC5B. We used CRISPR interference to invalidate UNC5B in HCC1937 breast cell line and grafted in mice and observed that the absence of UNC5B completely altered the ability to initiate tumors (**Supp. Fig. 3H**). Together, these data strongly support the idea that netrin-1/UNC5B blockade has a specific impact on CSCs/TICs and prevents recurrence/resistance of breast and ovary tumors after chemotherapy.

Netrin-1 blockade alleviates resistance to immune checkpoint inhibitor therapy.

Based on the impact on CSCs/TICs described here and the existing literature on cancer stemness, plasticity and resistance to immunotherapy[24,36], we next investigated whether netrin-1 blockade might also attenuate tumor resistance to immune checkpoint inhibitor (ICPI). For this we used the mouse mammary tumor cell line EMT6, which expresses netrin-1(**Supp. Fig. 4A)** and has some susceptibility to anti-CTLA-4[37,38]. This model demonstrates a ~35% of tumor growth inhibition when treated with anti-CTLA-4 (**Supp. Fig. 4B**), though spaghetti curves indicate that it acts

as an on/off model where mice may respond or not. About 60% of mice are non-responders (**Supp. Fig. 4C**). This heterogeneity is highlighted by individual animal-specific cytokine secretion profiles, which reveals "cold" and "hot" animals in terms of immune response (**Supp. Table 4**).

Consistent with anti-CTLA4 activity, the level of regulatory T (T-reg) cells[39], was downregulated in all mice, but less than 40% of mice demonstrated modulation of tumor growth (**Supp. Fig.4D**). Anti-netrin-1 mAb was unable to significantly inhibit tumor growth at all, when used as a single agent (**Supp. Fig. 4E**). However, the combination of anti-netrin-1 with anti-CTLA-4 dramatically blocked tumor growth, and strongly enhanced the long-term survival of mice bearing EMT6 tumors (**Fig. 4A-B**). This increased response to the anti-CTLA-4 mAb induced by netrin-1 blockade was associated with increased secretion of pro-inflammatory cytokines such as IFNγ (**Supp. Fig. 4F**), suggesting a robust immune response[24,40].

In parallel studies, we analyzed the tumor immune infiltrate using both lymphoid and myeloid panels by flow cytometry. We noticed an increase of $CD8^+$ T lymphocytes within tumors of mice treated with the combination of both antibodies, supporting the notion that immune cell populations promote the enhanced anti-tumor effect observed (**Fig. 4C-D**). In addition to T cell response, we analyzed the regulation of innate immunity. A decrease in tumor associated macrophages was observed within tumors of mice treated with the combination anti-netrin-1/anti-CTLA-4, supporting the view that these immune cell populations promote the enhanced anti-tumor effect observed (**Fig. 4E**).

PMN-MDSCs participate to netrin-1 mediated cancer stem cell enrichment and resistance to immune checkpoint inhibitors.

To explore the underlying mechanisms linking immune infiltration and its possible link with the anti-netrin-1 response, we next analyzed immune subpopulations known to be involved in resistance to immune checkpoint inhibitors. We identified, in the EMT6 engrafted model, a specific decrease in PMN-MDSCs[41], a subtype of myeloid-derived suppressor cells (MDSCs) derived from the neutrophil/polymorphonuclear compartment ($CD11b^+$ $Ly6G^+$ $Ly6C^{Interm}$) within tumors treated with anti-netrin-1 **(Fig.5A)**. The same population was found to be down-regulated upon anti-netrin-1 mAb treatment in a spontaneous genetic breast cancer

model MMTV/NeuT. These mice spontaneously develop mammary tumors closed to human pathology[42] **(Fig.5B)**.

MDSCs have been reported to be able to control and protect cancer stem cell populations[43]. PMN-MDSCs are immature cells capable of inhibiting the functions of T cells. They can accumulate during tumor growth and contribute to cancer development[41]. We thus hypothesized that these PMN-MDSCs could link the effect of netrin-1 interference on the tumor microenvironment and the resistance to treatments mediated by CSCs/TICs. To analyze *in vivo* the MDSC function, we differentiate immature myeloid cells into PMN-MDSCs. These immature myeloid cells were purified from bone marrow of wild type mice and differentiated into PMN-MDSCs by treatment with IL-6 and GM-CSF, that we reinjected into EMT6 tumor, treated with anti-netrin-1 and anti-CTLA-4. As a result, injection of PMN-MDSCs inhibit the effect of the combo-therapy highlighting the immuno-suppressive role of these cells **(Fig. 5C)**. To analyze if PMN-MDSCs can directly impact on CSCs, we evaluated their impact on $CD49f^{High}$ populations in a coculture model with EMT6 cells in which netrin-1 had been silenced. As shown in **Figure 5D**, we observed that PMN-MDSCs sustained the $CD49f^{+}$ stem EMT6 cell population, an effect that was lost when netrin-1 was silenced. *In vitro*, PMN-MDSCs inhibit $CD3^{+}$ T-cell proliferation and IFNγ production concomitant with the activation of cytotoxic $CD8^{+}$ lymphocytes, which clearly demonstrates their immunosuppressive roles in this context **(Supp. Fig.5A-B)**.

To determine whether the potentiation of the anti-CTLA-4 response by netrin-1 blockade was related to the impact of netrin-1 interference on CSCs/TICs, we analyzed stemness markers in EMT6 tumors treated either with anti-netrin-1 mAb alone or in combination with anti-CTLA-4. By selecting $CD45^{-}$ non-immune cells that were either $CD49f^{+}$ or $CD326^{-}$ (murine stemness markers[26]), we found that systemic anti-CTLA-4 treatment was associated with an enhancement of the stem cell populations (**Fig. 5E**; **Supp. Fig. 5C**). This suggests that the anti-CTLA-4 antibody principally affects bulk tumor cells, thus leaving residual tumors enriched for CSCs/TICs responsible for tumor recurrence. Moreover, we quantified at the same time point PMN-MDSCs cells by immunohistochemistry analysis (flow cytometry analysis was not possible due to a high rate of necrosis linked to CTLA-4 cytotoxic activity). We show that $Ly6G^{+}$ cells are decreased both in the monotherapy with anti-netrin-1 mAb and in the combo with anti-CTLA-4, arguing in a protective role of these cell for CSCs (**Fig. 5F**).

We also assessed cancer stem cell function by performing a serial transplantation assay comparing anti-netrin-1, anti-CTLA-4, or the combination. As shown in **Figure 5G**, while treatment with anti-netrin-1 or its combination with anti-CTLA-4 completely abolished tumor take in serially transplanted mice, treatment with anti-CTLA-4 only modestly inhibited tumor take. These data extend a literature which notes that ICPIs only partially impact cancer stem cell populations[24]. Of major interest, the combination of anti-CTLA-4 and anti-netrin-1 completely inhibits the enrichment in these stem cell populations associated with anti-CTLA-4 antibody, making it a promising strategy.

To further link our observations on cell subpopulations expressing stem cell markers and CSC/TIC function, we sorted cells using CD49f and CD326 markers from untreated EMT6 transplanted tumors and then transplanted them serially. As might be predicted, we found that $CD49f^+$ or $CD326^-$ EMT6 cells were more prone to form tumors than their $CD49f^-$ and $CD326^+$ counterparts (**Supp. Fig. 5D-E**). Moreover, $CD49f^+$ cells sorted from tumors treated with anti-netrin-1 mAb are losing their enhanced ability to form new tumors in serial transplantation assays (**Fig. 5H**). To unravel the mechanism behind, this effect we observed that while the *In vitro* treatment of EMT6 cells with anti-netrin-1 mAb leads to the decrease of $CD49f^+$ cells (**Supp. Fig. 5F**), this decreased is reverted when the general caspase inhibitor BOC was added **(Supp. Fig. 5F**)., supporting further the view that netrin-1 blockade impacts on CSCs by affecting cell death, In order to demonstrate the role of the receptor in these experiments, we invalidate UNC5B by shRNA in EMT6 and identified that the knock-down of UNC5B altered the ability to initiate tumors in mice (**Supp. Fig. 5G**). Collectively, our data support the view that the combination of ICPI and anti-netrin-1 is sensitizing grafted tumors to ICPI by the impact of the anti-netrin-1 mAb on cancer stem cell populations supported by the tumoral microenvironment.

Discussion

The present data identifies, for the first-time, netrin-1 as an independent progression factor in breast and high grade serous ovarian cancers, associated with a higher expression in CSCs/TICs. We show that netrin-1 interference may not only drive tumor growth inhibition but may also be important in the prevention of tumor relapse as well as in resistance to chemotherapy or immunotherapy. In support of this notion, we identified that targeting netrin-1 in association with standard of care chemotherapies induced a significant extension of the tumor-free survival (associated with a delay in tumor relapse) in animal models of both breast and high grade ovarian serous carcinoma. Similarly, we have shown that resistance to the ICPI anti-CTLA-4 could be alleviated by the association with the anti-netrin-1 mAb.

A challenging question remains; to understand the molecular mechanisms inhibited or unleashed upon netrin-1 blockade that confer relapse delay and/or alleviate resistance. We propose here that netrin-1 may play a specific role in CSCs/TICs since (i) netrin-1 is often specifically more expressed in CSCs/TICs compared to bulk tumor cells and (ii) netrin-1 blockade appears to reduce CSCs/TICs -*i.e.*, monitored using both functional assays or markers. Although netrin-1 was initially considered as a guidance cue, several recent published works seem to describe a role of netrin-1 in induced pluripotent stem cells, embryonic stem cells and naïve pluripotency[44–46]. The link between normal and embryonic stemness has not been extended to cancer "stemness," a prior *in vitro* study reported a possible role of netrin-1 in glioblastoma CSCs[8]. Based on an initial work from our lab, netrin-1 has been described as a survival factor in iPSC and ES, and acts in part by blocking the death induced by the dependence receptor UNC5B[44]. More recent work suggests that netrin-1 also links the Wnt and MAPK pathways[45]. Whether the biology behind "normal" stemness and CSCs/TICs relies on similar mechanisms should now be examined. Similarly, whether the reduction of CSCs/TICs associated with netrin-1 blockade seen in this manuscript is related to increased cell death or "lineage" commitment remains to be investigated. Nonetheless, our work, for the first time, links netrin-1 to breast and ovarian cancer progression and suggests it to be a *bona fide* clinical target. Based on these studies, a phase 2 clinical trial (https://clinicaltrials.gov/ct2/show/NCT04652076) was started in

late 2020 combining anti-netrin-1 and standard of care chemotherapy as well as immunotherapy.

The data obtained with the combination of ICPI with the anti-netrin1 mAb are of specific importance taken into account the currently limited clinical activity of ICPI in breast cancer [37,38]. The data presented here support the view that the suppression of ICPI resistance by netrin-1 blockade is associated with its impact on CSCs/TICs. However, we cannot yet exclude others additional mechanisms. Moreover, previous works have described the role of netrin-1 in the migration or the survival of immune cells such as macrophage[4–7] or $CD4^+$ cells[47] during inflammatory arthritis or obesity. MDSCs have already been reported to modulate the response to ICPI drugs[41,48].

PMN-MDSCs have already been shown to be capable of sustaining tumor progression[41]. In our investigations, we identify that netrin-1 blockade silences these cells. We propose a novel pro-tumoral effect of immune cells, sustain CSCs/TICs and thus may indirectly affect resistance to treatment. This proposed mechanism is consistent with a mechanism in which the potentiation of ICPI by netrin-1 blockade does not necessarily occur through direct reinforcement of immune effector cells but rather through an indirect effect on CSCs/TICs. We thus propose that netrin-1 produced by cancer cells sustains PMN-MDSC which in turn sustains CSCs/TICs that contribute to both recurrence and to resistance to chemotherapies and ICPIs.

However it is fair to say it probably includes additional players of the tumor microenvironment more generally impacting on tumoral plasticity such as CAFs[49], additional immune cells, endothelial cells, and extracellular matrix but also more generally the cellular stress reported in tumoral and stromal cells[25]. Whether and how netrin-1 might interact with these additional players remains an open question.

Materials and Methods:

Ethics, Human tumors samples and biological annotations:

The usage of all patient tumor samples was supported according to French regulations on the protection of biomedical investigation subjects. The collection of human samples was realized with primary female breast tumors from patients treated at the Centre Léon Bérard, conserved in the Centre des Ressources Biologiques (CRB) of the Centre Léon Bérard. Informed consent was obtained from all patients, and the study use samples which were approved by the ethics committee of the institutions. Fresh samples were addressed for mammosphere formation experiments, frozen tissues for q-RT-PCR analysis and fixed tissues to immunohistochemistry.

Cell culture

All the cell lines were obtained from ATCC. Murine mammary carcinoma EMT-6 cells were cultured in Eagle's Minimum Essential Medium (EMEM, ATCC) complemented with 10% of Serum Foetal Bovine (FBS, Gibco) and antibiotics (Streptomycin and Penicillin). They were cultured in Dulbecco's Modified Eagle's Medium (DMEM) for SKBR7 and Hs578t or RPMI for BT474, T47D, MDA-MB468, OV90 and OVCAR3, complemented with 10% FBS (Gibco) and antibiotics. HCC1937 cell line was cultured in RPMI complemented with 10% FBS (Gibco), 2% Na Bicarbonate, 1% Na Pyruvate, I% HEPES and antibiotics. Cells were maintained in culture at 37°C under humidified atmosphere consisting of 20% O_2 and 5% CO2. For the CRISPRi mediated silencing of hUNC5B in HCC1937 cell line, a small guide RNA (sgRNA) targeting hUNC5B promoter was designed using the sgRNA designer tool (https://portals.broadinstitute.org/gpp/public/analysis-tools/sgrna-design-crisprai). A control sgRNA targeting Firefly luciferase was also designed. Sequences are as follows: sgUNC5B: 5'- GCGCGCCTCTCGGAGCCCCG -3' and sgLUC: 5'-CGCCCACGGCCCTTCCCGGG-3'. Forward and reverse sgRNA-coding oligos with Esp3I linkers were ordered from Eurofins Genomics and then annealed by incubation

for 3 min at 90°C and 15 min at 37°C and ligated in pLV hU6-sgRNA hUbC-dCas9-KRAB-T2a-Puro [50] Insertion of sgRNA was confirmed by sequencing. The use of pLV hU6-sgRNA hUbC-dCas9-KRAB-T2a-Puro allows for the simultaneous expression of dCas9-KRAB and sgRNA and for selection for puromycin resistance. pLV hU6-sgRNA hUbC-dCas9-KRAB-T2a-Puro was a gift from Charles Gersbach (Addgene plasmid # 71236; http://n2t.net/addgene:71236 ; RRID:Addgene_71236). For the shRNA mediated KO of mUNC5B in EMT6 cell line, a pLKO.1-puro vector encoding shRNA targeting mUNC5B (Clone ID: TRCN0000072079, shRNA sequence: 5'-CGCCTACATCGTAAAGAACAA-3') was purchased from Sigma-Aldrich. Production of VSV-g pseudotyped lentivirus was made as described previously.

***In vivo* mice models and materials**:

Human anti-netrin-1 monoclonal antibodies (anti-netrin1) were supplied by Netris Pharma (Lyon, France). Female Swiss nude mice, 6-weeks old, were purchased from Charles River laboratories (Les Oncins, France) and maintained in specific pathogen-free conditions (Anican, Lyon, France) and stored in sterilized filter-topped cages. Their care and housing were in accordance with institutional European guidelines as put forth by the CECCAP local Ethical Committee (C2EA-15, CLB_2014_001; CLB_2014_012; CECCAPP_CLB_2016_017). The human human triple negative breast cancer patient derived xenograft PDX HBC146 was established and characterized for tumor recurrence by Marangoni *et al*[83]. The human triple negative breast cancer patient derived xenograft BRE-012 was established by the IMODI consortium(https://imodi-cancer.org/fr/). PDX-OV21 human high grade serous ovarian carcinoma model has been established by Curie Institute and previously published[51].

For PDX experiments, mice were grafted as described by Marangoni et al, 2007[24]. Tumor growth was evaluated by measurement of two perpendicular diameters of tumors with a caliper twice per week. Individual tumor volumes were calculated as V = (length*width^2)/2., a being the largest diameter, b the smallest. When tumors reached a volume of 300mm^3, the mice were randomly separated in two groups and submitted

anti-netrin-1 or Control alone, or in combination to standard or care chemotherapy: Adriamycin, 2 mg/kg (Doxorubicin, Teva Pharmaceuticals), and cyclophosphamide, 100 mg/kg (Endoxan, Baxter) were inoculated with a single i.p. injection or Carboplatin 66 mg/Kg (generic provided by Hospira) and Paclitaxel 30 mg/Kg (generic provided by Hospira), i. p. injection once a week Anti-netrin-1 mAb or IgG1 control were i.p. injected with 10mg/kg twice per week for the rest of the experiment. Animal work has been done by Netris pharma, Institut Curie or the Laboratoire des Modèles Tumoraux (LMT). 5 x 10^6 OV90 and OVCAR3 cells were subcutaneously inoculated with Matrigel (Corning) in the dorsal flank of 8-week-old female Swiss/Nude mice. The mice were housed under specific pathogen free (SPOF) conditions (Anican, Lyon, France). Tumor volumes were evaluated approximately every 3 days after initial detection using calliper[52]

For experiments of immune checkpoints inhibitors, eight-week-old (20-22 g body weight) female BalbC/J mice were obtained from Janvier Labs. 1 x 10^6 EMT-6 cells were subcutaneously inoculated in the dorsal flank of 8-week-old female BALB/cJ wild-type mice. The mice were housed under specific pathogen free (SPF) conditions as previously described (Anican, Lyon, France)[53]. Tumor volumes were evaluated approximately every 2 days after initial detection using calliper[52]. Based on initial intra-group homogeneity of tumor size, four different treatments have been administrated: IgG1 control isotype (Netris Pharma), anti-netrin-1 mAb (NP137, Netris Pharma) combination of anti-CTLA-4 mAb (BioXCell, Clone 9H10) with IgG1 and combination of anti-CTLA-4 with anti-netrin-1 mAb. The treatments were ip. administered respecting the following dose: 20 mg/kg anti-CTLA-4, 10 mg/kg anti-netrin-1 and 10 mg/kg mice IgG1 on days 8, 11 and 14 after the implant. Mice were sacrificed when individual tumours reached a predefined endpoint (1000-2000 mm^3).

For the injection of MDSCs cells, 500 000 EMT6 breast cancer cells were mixed with 50 000 PMN-MDSCs (ratio 10:1) produced *in vitro* and were inoculated in the dorsal flank of 8-week-old female BALB/cJ wild-type mice. Subsequently mice were intratumorally inoculated with PMN-MDSC at day 8 and 13.

Serial transplantation, tumor-initiating cell sorting and mammosphere culture: Tumors were dissociated with a collagenase (Sigma Aldrich) / DNAse (Life Technologies) for 45 minutes at 37°C, submitted to red blood cell lysis (Miltenyi Biotech) and passed through a 30 µm filter to obtain a single cell suspension. Cell viability has been evaluated by trypan blue count under the microscope to ensure the engraftment of the same number of cells with a similar viability in the different conditions of treatment, residual cells were after analyzed and sorted by FACS or submitted to mammosphere formation. FACS sorting was performed on a BD FACSDiVa. Anti-CD44-PE (BD system) was used to count and sort $CD44^{high}$ cells and dead cells were counted with propidium iodine staining. ALDEFLUOR (Stemcell Technologies) was used to count and sort $ALDH^{high}$ cells and dead cells were counted with propidium iodine staining. Mammosphere enrichments were obtained by culturing the cells on 6 wells ultra-low attachment dishes in mammocult medium (Stem cell technologies). Cells were allowed to form clonal mammospheres for 7 to 10 days of culture. For mammosphere forming assays, viable singlets were sorted by FACS and directly plated on 96 wells ultra-low attachment dishes at the density of 1000 cells per well in mammocult medium. Mammospheres were counted after 7 days of culture. To analyze spheres passages, 7 days spheres were dissociated and 1000 cells per well were again plated in the conditions mentioned above and counted after 7 days of culture.

Immunohistochemistry:

Immunohistochemistry analysis was performed on 4-µm-thick sections of paraffin embedded mouse tissues stained with anti-CD44 (156-3C11, Thermo Fisher) or anti-netrin-1 (CPA2389, Cohesion Biosciences) or anti-Ly-6G (E6Z1T- Rabbit mAb #87048 Cell signaling) dilution 1/500. Expressions are revealed by brown DAB staining. Nuclei are counterstained by hematoxylin (blue).

Flow cytometry analysis:

EMT6 subcutaneous tumors were mechanically disaggregated in RPMI-1640 medium 5% FBS and enzymatically digested with 1 mg/ml of collagenase I and 40 U/ml of DNAse I (Sigma Aldrich) for 30 min at 37 °C. Cells were passed through a 70 µm-cell strainer and filtered. After RBC lysis, cells were passed through a 30 µm-cell strainer and filtered. Cell pellets were resuspended in HBSS (Gibco) before counting. 2 x 10^6 cells were stained for the viability with Zombie Aqua (Biolegend) for 30 minutes at 4°C. Cells were washed and incubated with Fc Block purified anti-mouse CD16/CD32 (Clone 93, Biolegend), followed by staining with mouse anti-CD4 (RM4-5, Brilliant Violet 785), anti-CD19 (6D5, Brilliant Violet 605), anti-NKp46 (29A1.4, PE), anti-CD45 (30-F11, Alexa Fluor 700), anti-CD25 (PC61, APC), anti-CD69 (H1.2F3, FITC), anti-IA-IE (M5/114.15.2, BV421), anti-Ly6C (HK1.4, APC-Cy7) anti-Ly6G (1A8, FITC), CD11b (M1/70, BV785) and F4/80 (BM8, APC) from Biolegend and anti-CD3 (clone 500A2, PerCP-eFluor 710, anti-CD8b (eBioH35-17.2, eFluor 450), anti-CD44 (IM7, PerCP-Cy5.5), anti-CD326 (G8.8, PE-Dazzle 594) from eBioscience, anti-CD49f (GoH3, eFluor 450) from Life Technologies, for 45 min at 4 °C. Cells were fixed and permeabilized with the Foxp3 transcription factor staining buffer set (eBiosciences), and overnight stained for 30 min at 4 °C for IFN γ (XMG1.2, PE, Biolegend) and with anti-Foxp3 (FJK-16s, PE-Cyanine7, eBioscience). Analyses were performed with Fortessa HTS flow cytometer (BD Biosciences). Data were analyzed with FlowLogic Version 6 (Miltenyi Biotec, Germany). All gates were defined using fluorescence minus one control (FMO).

Cell isolation

$CD3^+$ T-cells were isolated from the Lymph nodes of 7-week-old BALB/cJ wild-type mice. The separation was performed by using Pan T Cell Isolation Kit (Miltenyi Biotech) and MACS column. Purity of cell population were evaluated by flow cytometry. $CD3^+$ T-cells were cultivated *in-vitro* for 3-days with Anti-CD3 and Anti-CD28 (Dynabeads, Gibco) and IL-2 (10 ng/ml). Immature myeloid cells were purified from bone marrow of

7-week-old BALB/cJ wild-type mice. Red blood cells (RBC) were lysate with ACK (Ammonium-Chloride-Potassium) Lysing Buffer, cells were filtered through a 70 µm-cell strainer. Immature myeloid cells were cultivated *in-vitro* for 4-days with GM-CSF and IL-6 (40ng/ml) to differentiate them. T-cells and PMN-MDSCs were cultivated in RPMI complemented with 10% FBS (Gibco), 1% Na Bicarbonate, 1% Na Pyruvate, 1% L-glutamine (Gibco), l% HEPES, 0.05 mM 2-mercaptoethanol (Gibco) and antibiotics.

Proliferation viability and cell death assays

$CD3^+$ T-cells were labeled with cell trace violet (CTV, Invitrogen) as follows: 10^6 cells were incubated with 1 µM of CTV in PBS for 20 min at 37°C, 5% CO2. 5-volume of culture medium were added, and cells were left at 37°C 5% CO2 in culture medium for additional 5 min. Cells were analyzed by flow cytometry for the proliferation baseline or co-cultured with PMN-MDSCs. WST1 assay was used according to the manufacturer (Cell proliferation Reagent, Roche) to measure cell viability. Cells are fixed in 70% Ethanol and stained with Propidium iodide (PI). SubG1 population is further identified by flow cytometry.

IFN-γ Production

Activated $CD3^+$ T-cells were stimulated with phorbol myristate acetate (PMA), Ionomycin, Brefeldin (Biolegend) and Monensin (Biolegend) for 4 hours at 37°C, 5% CO2 in complete culture medium. IFN γ released by $CD8^+$ T- cells was evaluated by flow cytometry.

Co-culture

To test the immunosuppressive activity of PMN-MDSCs were co-cultured with purified $CD3^+$ T-cells for 3 days at different ratio (MDSCs: $CD3^+$ T-cells, 1:1, 1:4) in 96-well plate. To analyze the effect PMN-MDSCs on stemness were co-cultured with EMT6-control vector EMT6-Sh netrin-1 in a ratio 1:10 (MDSCs: Tumoral cells) for 24 hours in

24 well plate. CD49f^{high} cells were analyzed by flow cytometry.

Cytokine analysis:

To measure the systemic release of IFNγ, fresh stabilized whole blood was drawn from BALB/cJ wild-type mice 16h hours after 1st, 2nd and 3rd treatments. Plasma was separated and used to measure the protein levels of IFN γ with the Mouse IFN-gamma Quantikine ELISA Kit (R&D System, Minnesota, USA) according to the manufacturer's instructions.

For cytokines array analysis, 31 cytokines and chemokines were analyzed 18 hours after the 2nd CTLA-4 treatment, using the multiplex assays manufactured by Meso Scale Discovery (MSD; Gaithersburg, MD). EMT6 subcutaneous tumors were mechanically disaggregated in 500μl of RPMI-1640 medium (in absence of FBS) for 500 mg of tumor. The cytokines and chemokines analyzed accordingly to the manufacturer recommandations and were IL-1β, IL-2, IL-4, IL-5, IL-6, IL-9, IL-10, IL-12p70, IL-15, IL-16, IL-17A, IL-17A/F, IL-17C, IL-17E/IL-25, IL-21, IL-22, IL-23, IL27p28/IL30, IL-31, IL-33, IFN γ, MIP-1α, MIP-2, MIP-3α, IP-10, MCP-1, KC/GRO, TNF-α, TGF- β2, TGF-β3, TGF-β1. Analyses were performed using the software Discovery workbench 4.0.

Immunoblots:

Confluent cells were washed with cold PBS and scrapped in lysis buffer (Tris 10 mM pH 7.6; SDS 5; Glycerol 10%; Triton X-100 1%, DTT 100mM). After sonication proteins were dosed using Pierce 660nm Protein Assay Reagent (Thermo Fisher Scientific) and after loading on 4%-15% SDS-polyacrylamide gels (Bio-Rad) transferred to nitrocellulose membranes using Trans-Blot Turbo Transfer (Bio-Rad). Membranes were blocked for 1 hour at room temperature with 5% of nonfat dried milk for the Netrin-1 and with 5% of BSA and 1% of nonfat dried milk for UNC5B. Staining was performed overnight with primary antibody: anti-netrin1 antibody (Ab126729, Abcam) and anti-UNC5B (D9M7Z, Cell signaling technology). After washing, membranes were

incubated with secondary antibody, goat anti-rabbit coupled with HRP for 1 hour at room temperature. West Dura Chemiluminescence System (Pierce) was used to intensify the signal. Imaging was performed using Chemidoch Touch (Bio-Rad). Full membrane westernblots were included in the supplementary material.

RNA expression analysis:

Total mRNAs were extracted from tissues or cells using Nucleospin RNAII kit (Macherey-Nagel) and 1 µg was reverse transcribed using the iScript cDNA Synthesis kit (Bio-Rad). Real-time quantitative RT–PCR was performed on a LightCycler 2.0 apparatus (Roche, Meylan, France) using the Light Cycler Master Taqman kit (Roche, Meylan, France). Oligonucleotide sequences are available upon request.

Statistical analysis:

To test netrin-1 expression, cohorts were dichotomized based on Netrin-1 median expression. Survival curves were produced by the Kaplan-Meier method on Prism (GraphPad Software, San Diego, California). Data were analyzed using a Mantel-Cox test. n defines the total number of replicates. All statistical tests were two-sided. The multivariate analysis was realized with COX model in the R software. Kaplan-Meier curves of disease-free survival of overall survival were analyzed with a Gehan-Breslow-Wilcoxon Test in the GraphPad Prism software.

For mice experiments, statistical methods were not used to predetermine necessary sample size, but sample size was chosen based on pilot experiments which applying appropriate statistical test could return significant results. Tumor growth with time was analyzed by two-way ANOVA with Bonferroni correction. Survival curves were analyzed using the Log-rank (Mantel-Cox) test. Flow cytometry data are reported as mean±s.e.m. in case of representative experiment; the pool of different experiments is expressed as a *ratio* of the control group of the single experiment. Statistical analysis was performed by Mann-Whitney test (GraphPad).

Acknowledgments:

We thank Dwayne Stupack for correction and helpful discussion, the LMT platform for the high quality of the animal work. This work was supported by Netris Pharma and institutional grants from CNRS (PM, BG), University of Lyon (PM), Centre Léon Bérard (PM) and from the Ligue Contre le Cancer (PM), INCA (PM), Euronanomed (PM, BG), ANR (PM), BMS Foundation for Immunotherapy (PM). AR received a 4th year fellowship from Ligue contre le Cancer.

Conflict of interest:

BD, CV, JL, DN, DG, SD, AB and PM declare to have a conflict of interest as respectively employees (BD, DN, DG, CV, JL and SD) and shareholders (AB and PM) of NETRIS Pharma.

Author contributions:

BD, ARR, CV, RC, RB, AP and JL performed the cell experiments and *in vitro* data;

BD, ARR, MH, PV, DN, MR, IG, FN and PAL performed mice experiments;

CV, RB, AP and DG produced the lentiviruses and CRISPR and Sh cell lines;

BD, AF, IT and NG made anatomopathological analysis;

NR performed bioinformatical analysis;

NG, IT, IRC, EML, CG, STE and MDS provided human samples and cell lines;

BD, ARR and SC performed statistical analysis;

BD, SD, DD, EM, KJM, BG, PM and AB have participated to the research design and to write the paper.

Data Availability statement:

Data sharing not applicable to this article as no datasets were generated or analysed during the current study.

References:

1 Serafini T, Colamarino SA, Leonardo ED, Wang H, Beddington R, Skarnes WC *et al.* Netrin-1 Is Required for Commissural Axon Guidance in the Developing Vertebrate Nervous System. *Cell* 1996; **87**: 1001–1014.

2 Chédotal A. Roles of axon guidance molecules in neuronal wiring in the developing spinal cord. *Nat Rev Neurosci* 2019; **20**: 380–396.

3 Mehlen P, Delloye-Bourgeois C, Chédotal A. Novel roles for Slits and netrins: axon guidance cues as anticancer targets? *Nat Rev Cancer* 2011; **11**: 188–197.

4 Mehlen P, Bredesen DE. Dependence receptors: from basic research to drug development. *Sci Signal* 2011; **4**: mr2.

5 Bongo JB, Peng DQ. The neuroimmune guidance cue netrin-1: a new therapeutic target in cardiovascular disease. *J Cardiol* 2014; **63**: 95–98.

6 van Gils JM, Derby MC, Fernandes LR, Ramkhelawon B, Ray TD, Rayner KJ *et al.* The neuroimmune guidance cue netrin-1 promotes atherosclerosis by inhibiting the emigration of macrophages from plaques. *Nat Immunol* 2012; **13**: 136–143.

7 Ramkhelawon B, Hennessy EJ, Ménager M, Ray TD, Sheedy FJ, Hutchison S *et al.* Netrin-1 promotes adipose tissue macrophage retention and insulin resistance in obesity. *Nat Med* 2014; **20**: 377–384.

8 Sanvoranart T, Supokawej A, Kheolamai P, U-pratya Y, Poungvarin N, Sathornsumetee S *et al.* Targeting Netrin-1 in glioblastoma stem-like cells inhibits growth, invasion, and angiogenesis. *Tumor Biol* 2016; **37**: 14949–14960.

9 Barnault R, Verzeroli C, Fournier C, Michelet M, Redavid AR, Chicherova I *et al.* Hepatic inflammation elicits production of proinflammatory netrin-1 through exclusive activation of translation. *Hepatology* 2022; : hep.32446.

10 Fazeli A, Dickinson SL, Hermiston ML, Tighe RV, Steen RG, Small CG *et al.* Phenotype of mice lacking functional Deleted in colorectal cancer (Dcc) gene. *Nature* 1997; **386**: 796–804.

11 Leonardo ED, Hinck L, Masu M, Keino-Masu K, Ackerman SL, Tessier-Lavigne M. Vertebrate homologues of C. elegans UNC-5 are candidate netrin receptors. *Nature* 1997; **386**: 833–838.

12 Gibert B, Mehlen P. Dependence Receptors and Cancer: Addiction to Trophic Ligands. *Cancer Research* 2015; **75**: 5171–5175.

13 Fitamant J, Guenebeaud C, Coissieux M-M, Guix C, Treilleux I, Scoazec J-Y *et al.* Netrin-1 expression confers a selective advantage for tumor cell survival in metastatic breast cancer. *Proceedings of the National Academy of Sciences* 2008; **105**: 4850–4855.

14 Delloye-Bourgeois C, Fitamant J, Paradisi A, Cappellen D, Douc-Rasy S, Raquin M-A *et al.* Netrin-1 acts as a survival factor for aggressive neuroblastoma. *J Exp Med* 2009; **206**: 833–847.

15 Delloye-Bourgeois C, Brambilla E, Coissieux M-M, Guenebeaud C, Pedeux R, Firlej V *et al.* Interference with netrin-1 and tumor cell death in non-small cell lung cancer. *J Natl Cancer Inst* 2009; **101**: 237–247.

16 Paradisi A, Creveaux M, Gibert B, Devailly G, Redoulez E, Neves D *et al.* Combining chemotherapeutic agents and netrin-1 interference potentiates cancer cell death. *EMBO Mol Med* 2013; **5**: 1821–1834.

17 Grandin M, Meier M, Delcros JG, Nikodemus D, Reuten R, Patel TR *et al.* Structural Decoding of the Netrin-1/UNC5 Interaction and its Therapeutical Implications in Cancers. *Cancer Cell* 2016; **29**: 173–185.

18 Kryza D, Wischhusen J, Richaud M, Hervieu M, Sidi Boumedine J, Delcros J

et al. From netrin-1-targeted SPECT / CT to internal radiotherapy for management of advanced solid tumors. *EMBO Mol Med* 2023; **15**: e16732.
19 Cassier P, Eberst L, Garin G, Courbebaisse Y, Terret C, Robert M *et al.* A first in human, phase I trial of NP137, a first-in-class antibody targeting netrin-1, in patients with advanced refractory solid tumors. *Annals of Oncology* 2019; **30**: v159.
20 Cassier PA, Navaridas R, Bellina M, Rama N, Ducarouge B, Hernandez-Vargas H *et al.* Netrin-1 blockade inhibits tumour growth and EMT features in endometrial cancer. *Nature* 2023. doi:10.1038/s41586-023-06367-z.
21 Lengrand J, Pastushenko I, Vanuytven S, Song Y, Venet D, Sarate RM *et al.* Pharmacological targeting of netrin-1 inhibits EMT in cancer. *Nature* 2023. doi:10.1038/s41586-023-06372-2.
22 Reya T, Morrison SJ, Clarke MF, Weissman IL. Stem cells, cancer, and cancer stem cells. *Nature* 2001; **414**: 105–111.
23 Yeung TM, Gandhi SC, Wilding JL, Muschel R, Bodmer WF. Cancer stem cells from colorectal cancer-derived cell lines. *Proc Natl Acad Sci USA* 2010; **107**: 3722–3727.
24 Miao Y, Yang H, Levorse J, Yuan S, Polak L, Sribour M *et al.* Adaptive Immune Resistance Emerges from Tumor-Initiating Stem Cells. *Cell* 2019; **177**: 1172-1186.e14.
25 Lu H, Xie Y, Tran L, Lan J, Yang Y, Murugan NL *et al.* Chemotherapy-induced S100A10 recruits KDM6A to facilitate OCT4-mediated breast cancer stemness. *Journal of Clinical Investigation* 2020. doi:10.1172/JCI138577.
26 Batlle E, Clevers H. Cancer stem cells revisited. *Nat Med* 2017; **23**: 1124–1134.
27 Ye L, Lin C, Wang X, Li Q, Li Y, Wang M *et al.* Epigenetic silencing of SALL 2 confers tamoxifen resistance in breast cancer. *EMBO Mol Med* 2019; **11**. doi:10.15252/emmm.201910638.
28 Arfaoui A, Rioualen C, Azzoni V, Pinna G, Finetti P, Wicinski J *et al.* A genome-wide RNA i screen reveals essential therapeutic targets of breast cancer stem cells. *EMBO Mol Med* 2019; **11**. doi:10.15252/emmm.201809930.
29 Junttila MR, de Sauvage FJ. Influence of tumour micro-environment heterogeneity on therapeutic response. *Nature* 2013; **501**: 346–354.
30 Papanastasiou AD, Pampalakis G, Katsaros D, Sotiropoulou G. Netrin-1 overexpression is predictive of ovarian malignancies. *Oncotarget* 2011; **2**: 363–367.
31 Ginestier C, Hur MH, Charafe-Jauffret E, Monville F, Dutcher J, Brown M *et al.* ALDH1 is a marker of normal and malignant human mammary stem cells and a predictor of poor clinical outcome. *Cell Stem Cell* 2007; **1**: 555–567.
32 Charafe-Jauffret E, Ginestier C, Iovino F, Tarpin C, Diebel M, Esterni B *et al.* Aldehyde dehydrogenase 1-positive cancer stem cells mediate metastasis and poor clinical outcome in inflammatory breast cancer. *Clin Cancer Res* 2010; **16**: 45–55.
33 Marangoni E, Lecomte N, Durand L, de Pinieux G, Decaudin D, Chomienne C *et al.* CD44 targeting reduces tumour growth and prevents post-chemotherapy relapse of human breast cancers xenografts. *Br J Cancer* 2009; **100**: 918–922.
34 Dumartin L, Quemener C, Laklai H, Herbert J, Bicknell R, Bousquet C *et al.* Netrin-1 mediates early events in pancreatic adenocarcinoma progression, acting on tumor and endothelial cells. *Gastroenterology* 2010; **138**: 1595–1606, 1606.e1–8.
35 Grandin M, Meier M, Delcros JG, Nikodemus D, Reuten R, Patel TR *et al.* Structural Decoding of the Netrin-1/UNC5 Interaction and its Therapeutical Implications in Cancers. *Cancer Cell* 2016; **29**: 173–185.
36 Dongre A, Rashidian M, Reinhardt F, Bagnato A, Keckesova Z, Ploegh HL *et*

al. Epithelial-to-Mesenchymal Transition Contributes to Immunosuppression in Breast Carcinomas. *Cancer Res* 2017; **77**: 3982–3989.
37 Bayraktar S, Batoo S, Okuno S, Glück S. Immunotherapy in breast cancer. *J Carcinog* 2019; **18**: 2.
38 Polk A, Svane I-M, Andersson M, Nielsen D. Checkpoint inhibitors in breast cancer – Current status. *Cancer Treatment Reviews* 2018; **63**: 122–134.
39 Read S, Greenwald R, Izcue A, Robinson N, Mandelbrot D, Francisco L *et al.* Blockade of CTLA-4 on CD4 $^{+}$ CD25 $^{+}$ Regulatory T Cells Abrogates Their Function In Vivo. *J Immunol* 2006; **177**: 4376–4383.
40 Ni L, Lu J. Interferon gamma in cancer immunotherapy. *Cancer Med* 2018; **7**: 4509–4516.
41 Zhou J, Nefedova Y, Lei A, Gabrilovich D. Neutrophils and PMN-MDSC: Their biological role and interaction with stromal cells. *Seminars in Immunology* 2018; **35**: 19–28.
42 Guy CT, Webster MA, Schaller M, Parsons TJ, Cardiff RD, Muller WJ. Expression of the neu protooncogene in the mammary epithelium of transgenic mice induces metastatic disease. *Proceedings of the National Academy of Sciences* 1992; **89**: 10578–10582.
43 Peng D, Tanikawa T, Li W, Zhao L, Vatan L, Szeliga W *et al.* Myeloid-Derived Suppressor Cells Endow Stem-like Qualities to Breast Cancer Cells through IL6/STAT3 and NO/NOTCH Cross-talk Signaling. *Cancer Res* 2016; **76**: 3156–3165.
44 Ozmadenci D, Féraud O, Markossian S, Kress E, Ducarouge B, Gibert B *et al.* Netrin-1 regulates somatic cell reprogramming and pluripotency maintenance. *Nat Commun* 2015; **6**: 7398.
45 Huyghe A, Furlan G, Ozmadenci D, Galonska C, Charlton J, Gaume X *et al.* Netrin-1 promotes naive pluripotency through Neo1 and Unc5b co-regulation of Wnt and MAPK signalling. *Nat Cell Biol* 2020; **22**: 389–400.
46 Renders S, Svendsen AF, Panten J, Rama N, Maryanovich M, Sommerkamp P *et al.* Niche derived netrin-1 regulates hematopoietic stem cell dormancy via its receptor neogenin-1. *Nat Commun* 2021; **12**: 608.
47 Boneschansker L, Nakayama H, Eisenga M, Wedel J, Klagsbrun M, Irimia D *et al.* Netrin-1 Augments Chemokinesis in CD4+ T Cells In Vitro and Elicits a Proinflammatory Response In Vivo. *J Immunol* 2016; **197**: 1389–1398.
48 Lu W, Yu W, He J, Liu W, Yang J, Lin X *et al.* Reprogramming immunosuppressive myeloid cells facilitates immunotherapy for colorectal cancer. *EMBO Mol Med* 2021; **13**. doi:10.15252/emmm.202012798.
49 Sung P-J, Rama N, Imbach J, Fiore S, Ducarouge B, Neves D *et al.* Cancer-Associated Fibroblasts Produce Netrin-1 to Control Cancer Cell Plasticity. *Cancer Res* 2019; **79**: 3651–3661.
50 Thakore PI, D'Ippolito AM, Song L, Safi A, Shivakumar NK, Kabadi AM *et al.* Highly specific epigenome editing by CRISPR-Cas9 repressors for silencing of distal regulatory elements. *Nat Methods* 2015; **12**: 1143–1149.
51 Mieulet V, Garnier C, Kieffer Y, Guilbert T, Nemati F, Marangoni E *et al.* Stiffness increases with myofibroblast content and collagen density in mesenchymal high grade serous ovarian cancer. *Sci Rep* 2021; **11**: 4219.
52 Gibert B, Delloye-Bourgeois C, Gattolliat C-H, Meurette O, Le Guernevel S, Fombonne J *et al.* Regulation by miR181 family of the dependence receptor CDON tumor suppressive activity in neuroblastoma. *J Natl Cancer Inst* 2014; **106**. doi:10.1093/jnci/dju318.

53 Jiang S, Richaud M, Vieugué P, Rama N, Delcros J, Siouda M *et al.* Targeting netrin-3 in small cell lung cancer and neuroblastoma. *EMBO Mol Med* 2021. doi:10.15252/emmm.202012878.

Figure legends

Figure 1: Netrin-1 expression is a poor prognosis marker and correlates with stem cells marker in human breast and ovary cancers.

A-B. Kaplan-Meier curves representing the percentage of overall survival of breast cancer patients (**A**, n=89) or treatment-free survival among patients with localized disease (**B**, n=67). The cohort has been split in netrin-1 High (green) and Low (red) by the median expression in their tumors. **C.** Netrin-1 mRNA expression level within tumors segmented in High and Low by the median expression of CD44 mRNA (n=89). Bars are mean values +/- s.e.m. **D.** Netrin-1 mRNA expression level measured in fresh human tumors obtained at the diagnosis by q-RT-PCR. Each tumor was split to analyze the bulk or their corresponding derived mammospheres (Spheres, n=12) after dissociation. Bars are mean values +/- s.e.m. normalized with the tumor bulk group. **E-F.** Kaplan-Meier curves representing the percentage of overall survival (**E**) or treatment free survival (**F**) of high-grade ovarian carcinoma patients (n=51) with netrin-1 High (green), Low (red) Negative (black) expression in their tumors (Netrin-1 was measured by immunohistochemistry (IHC)). Median netrin-1 expression was used as a cutoff between groups. **G.** Boxplot presenting Allred score combining the percentage of positive cells and signal intensity of netrin-1 measured by IHC in patient's responder (n=17) *vs* resistant to platin treatment (n=8). **H.** Netrin-1 mRNA expression level in tumors segmented on the CD44 mRNA expression from a cohort of High grade serous ovarian carcinomas (n=31). High and Low have been determined respectively by the upper and lower values separated by the median of mRNA expression measured by q-RT-PCR. Bars are mean values +/- s.e.m. In all panels statistics are presented as * $p<0.05$; ** $p<0.01$.

Figure 2: Netrin-1 expression is associated with CSCs in human cell lines and in a PDX model of breast cancer resistance to chemotherapy.

A. Netrin-1 mRNA expression level was measured by q-RT-PCR in HS578t (n=3) or SKBR7 (n=3) cell lines treated 48h with 1 µM Adriamycin (Adria). Bars are mean values +/- s.e.m., normalized with the control group. **B**. Netrin-1 mRNA expression level was

measured by q-RT-PCR in BT474 (n=4 *vs* 5) or Hs578t (n=5) cell lines comparing standard 2D culture and mammosphere (Sphere) 3D. Bars are mean values +/- s.e.m., normalized with the control 2D group. **C.** Netrin-1 mRNA expression level was measured by q-RT-PCR in CD49f^{low} and CD49f^{high} Hs578t (n=4) sorted breast cell population and in CD44^{low} and CD44^{high} OV90 ovary cell line (n=6 *vs* 3). Bars are mean values +/- s.e.m., normalized with the control Low group**. D.** Tumor volume was measured along the different phases of the HBC146 PDX breast cancer model[33] treated with chemotherapy Adriamycin-Cyclophosphamide (AC): Growth, Regression, Remission and Relapse (n=20). Samples were collected at the different phases (red circles). **E.** Netrin-1 and CD44 mRNA expression levels were measured by q-RT-PCR in the different phases (untreated n=8, regression n=8 and relapse n=10). Bars are mean values +/- s.e.m., normalized with the untreated group. **F**. Percentage of CD44^{high} cells counted by FACS analysis in untreated tumors compared to regressing tumors (n=9 *vs* 3). **G**. Number of mammospheres formed by 1000 viable cells isolated from untreated HBC146 tumors or at the regression phase (n=5 *vs* 9). Bars are mean values +/- s.e.m. **H.** Netrin-1 mRNA expression level measured by q-RT-PCR in untreated bulk tumors and mammospheres (n=7). Bars are mean values +/- SEM, normalized to the bulk tumor group. **I.** SubG1 cell present in Hs578t cell line treated with siRNA control (siCtr) or siRNA against Netrin-1(siNtn-1) (n=3). **J.** Cell viability measured by WST1 assay in SKBR7 (n=3) cell lines treated with siCtr and siNetrin-1 alone or in combination with Adriamycin. Bars are mean values +/- SEM, normalized to the siCtr group (* are statistics against siCtr and $^{+}$ against siCtr + Adriamycin). **K.** Number of mammospheres formed by 1000 viable cells of Hs578t (n=5) and OV90 (n=3) cell lines treated with siCtr and siNetrin-1. Bars are mean values +/- SEM. In all panels statistics are presented as * p<0.05; ** p<0.01; $^{+++}$ or *** p<0.001.

Figure 3: Netrin-1 blockade delays cancer relapse and impact CSCs.

A. Tumor volume was measured along the different phases of the HBC146 PDX model: Growth, Regression after chemotherapy (Adriamycin-Cyclophosphamide: AC), Remission and Relapse. At day 21, the mice were randomized into two groups which were intraperitoneally treated either by vehicle (n=20) or with 10mg/kg of anti-netrin1 antibody weekly (n=20). p=0.0002 by ANOVA on the tumor volume at the regression. **B.** Kaplan-Meier curves representing the percent of mice free of relapse in vehicle

(green) and anti-netrin-1 mAb (red) treated groups. The relapse volume threshold has been determined at 40mm^3. Median of relapse are respectively 56.0 and 80.5 days after chemotherapy for the vehicle and anti-netrin-1 groups, p=0.0078 by Gehan-Breslow-Wilcoxon test. **C.** Number of mammospheres formed by 1000 viable cells (left) or viable PI negative cells (right) isolated from HBC146 tumors treated with chemotherapy alone or associated with anti-netrin-1 mAb. Samples were collected in regressing tumors, below the volume threshold of 40mm^3 (n=5 *vs* 9). Bars are mean values +/- s.e.m. **D.** Representative CD44 immunohistochemistry analysis of HBC146 tumors treated with chemotherapy alone or associated with the anti-netrin-1 mAb. Samples were collected in regressing tumors. Scale bar (represented by a line): 50µm. **E-F**. Serial transplantation experiments of HBC146 (n=10 per group) and BRE-012 (n= 10 per group) breast PDX. First, tumors were treated with the anti-netrin-1 mAb or with a control IgG1 and then regrafted in other mice. Secondary recipient were not treated after the re-engraftment, the percentage of mice free of tumor is presented in both groups. **G.** Tumor volume was measured in mice bearing the OV21 ovarian PDX model and treated with Carboplatin/Paclitaxel (CP) chemotherapy and randomly separated in two groups intraperitoneally treated either with control IgG1 (n=8) or with 10mg/kg of anti-netrin1 antibody (n=8). (p=0.0101; ANOVA test). **H-I**. Serial transplantation experiments of ovarian cancer cell lines OV90 (n=12) or OVCAR3 (n=8). First, grafted tumors were treated with the anti-netrin-1 mAb or with a IgG1 control and after dissociation, 1 x 10^6 living cells were regrafted in new recipient mice Results are presented as the percentage of mice free of tumor take with respectively. In all panels statistics are presented as * p<0.05; ** p<0.01; *** p<0.001.

Figure 4: Netrin-1 blockade alleviates resistance to immune checkpoint inhibitor anti-CTLA-4.

A. Tumor growth quantification of syngeneic EMT6 mammary carcinoma, in mice treated with control IgG1 or anti-netrin-1 mAb, in combination with anti-CTLA-4 mAb. **B**. Kaplan-Meier survival analysis of the mice of **A**. after 80 days. **C**. Spider graph presenting flow cytometry analysis of the immune infiltrate. All components of the lymphoid panel were detected and quantified after EMT6 tumor dissociation and isolation of cell population using Lymphocytes specific antibodies. **D**. Analysis of CD8$^+$ lymphocytes by flow cytometry infiltrating tumors treated with either anti-CTLA-4 mAb combined or not with anti-netrin-1 mAb and compared to a IgG1 control (n=17 per

group). Results are the mean of 2 different experiments presented in **C**. and are presented as a ratio on total $CD45^+$ cells singlets for each tumor. **E**. Analysis of tumor associated macrophages defined as $CD11b^+$ $LY6C^-$ $F4/80^+$ cells (n=16 per group). Results where the mean of 2 different experiments and are presented as a ratio on total $CD45^+$ cells singlets for each tumor. In all panels statistic are presented as * $p<0.05$; ** $p<0.01$.

Figure 5: Netrin-1 blockade efficiently impacts CSCs/TICs untargeted by anti-CTLA-4 mAb.

A-**B**. Flow cytometry analysis of PMN-MDSC obtained after dissociation of EMT6 (n=9 per group) or MMTV/NeuT (n=16 *vs* 19) tumors treated with either control isotype IgG1 or anti-netrin-1 mAb. PMN-MDSC are defined as $CD11b^+$ $Singlets^+$ cells among the $CD45^+$ ($CD11b^+$ $Ly6G^+$ $Ly6C^{interm}$) population. **C**. EMT-6 tumor implanted in syngeneic BALBc/J mice were treated with anti-netrin-1 and anti-CTLA4 and injected/not with PMN-MDSC cells. **D**. Flow cytometry analysis of $CD49f^+$ EMT6 cells in control parental cells, or netrin-1 silenced by shRNA (Sh netrin-1) cocultured, or not, with PMN-MDSC (n=3). **E**. Flow cytometry analysis of EMT6 cancer cells obtained after dissociation of tumors treated with either three treatments of control IgG1, anti-netrin-1 mAb alone or in combination with anti-CTLA-4 (respectively n=10, 8, 8 and 10). CSC markers are defined as $CD49f^+$ cells among the $CD45^{neg}$ ($CD45^-$) population. **F**. Immunohistochemistry analysis and quantification of $Ly6G^+$ cells in EMT6 obtained after fixation of tumors treated with either three treatments of control IgG1, anti-netrin-1 mAb with or without anti-CTLA-4. n=8 field/tumor. **G**. Serial transplantation experiments with EMT6 cells in syngeneic BALBc/J mice. 5.10^4 living cells, obtained after the dissociation of tumors from mice treated with either control IgG1 *vs*. anti-netrin-1 mAb alone; or in combination with anti-CTLA4 (respectively n=7, 8, 8 and 8) were grafted into recipient mice. Results are presented as percentage of mice free of tumor. **H**. Serial transplantation of EMT6 cells were used as an indicator of tumor initiating potential of $CD49f^{+/-}$ populations. Tumors were dissociated from EMT6 tumors of mice treated with control IgG1 or anti-netrin-1 mAb. After dissociation, cells were sorted based on CD49f expression and 5.10^4 living cells of each positive or negative populations were regrafted in new recipient animals (n=10 per group). Results are

presented as the percentage of mice free of tumor. In all panels statistics are presented as * $p<0.05$; ** $p<0.01$; *** $p<0.001$.

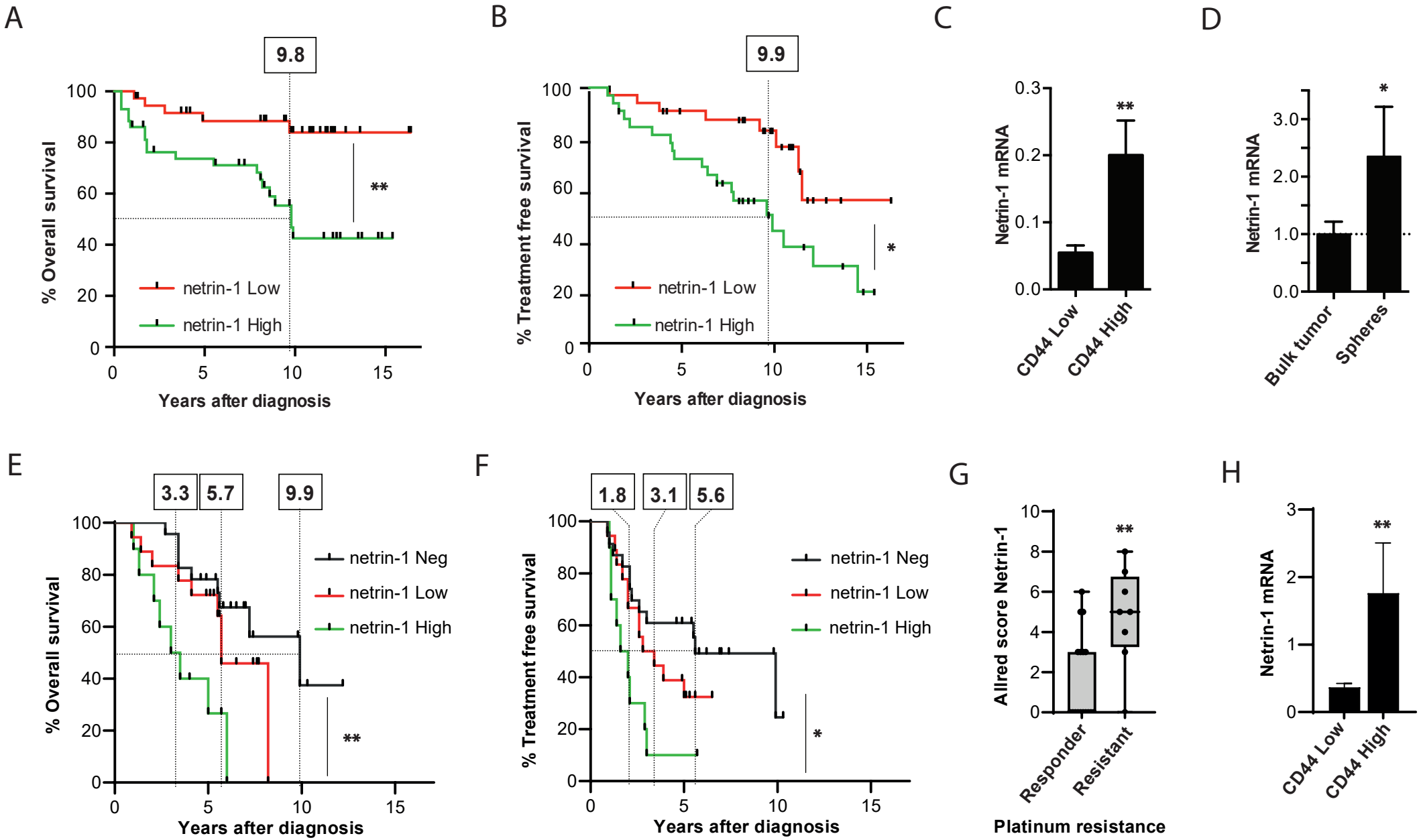
A
9.8
100
80
60
40
20
0
% Overall survival
netrin-1 Low
netrin-1 High
**
0
5
10
15
Years after diagnosis
B
9.9
% Treatment free survival
netrin-1 Low
netrin-1 High
*
Years after diagnosis
C
Netrin-1 mRNA
0.3
0.2
0.1
0.0
**
CD44 Low
CD44 High
D
Netrin-1 mRNA
3.0
2.0
1.0
0.0
*
Bulk tumor
Spheres
E
3.3
5.7
9.9
% Overall survival
netrin-1 Neg
netrin-1 Low
netrin-1 High
**
Years after diagnosis
F
1.8
3.1
5.6
% Treatment free survival
netrin-1 Neg
netrin-1 Low
netrin-1 High
*
Years after diagnosis
G
Allred score Netrin-1
10
8
6
4
2
0
**
Responder
Resistant
Platinum resistance
H
Netrin-1 mRNA
3
2
1
0
**
CD44 Low
CD44 High

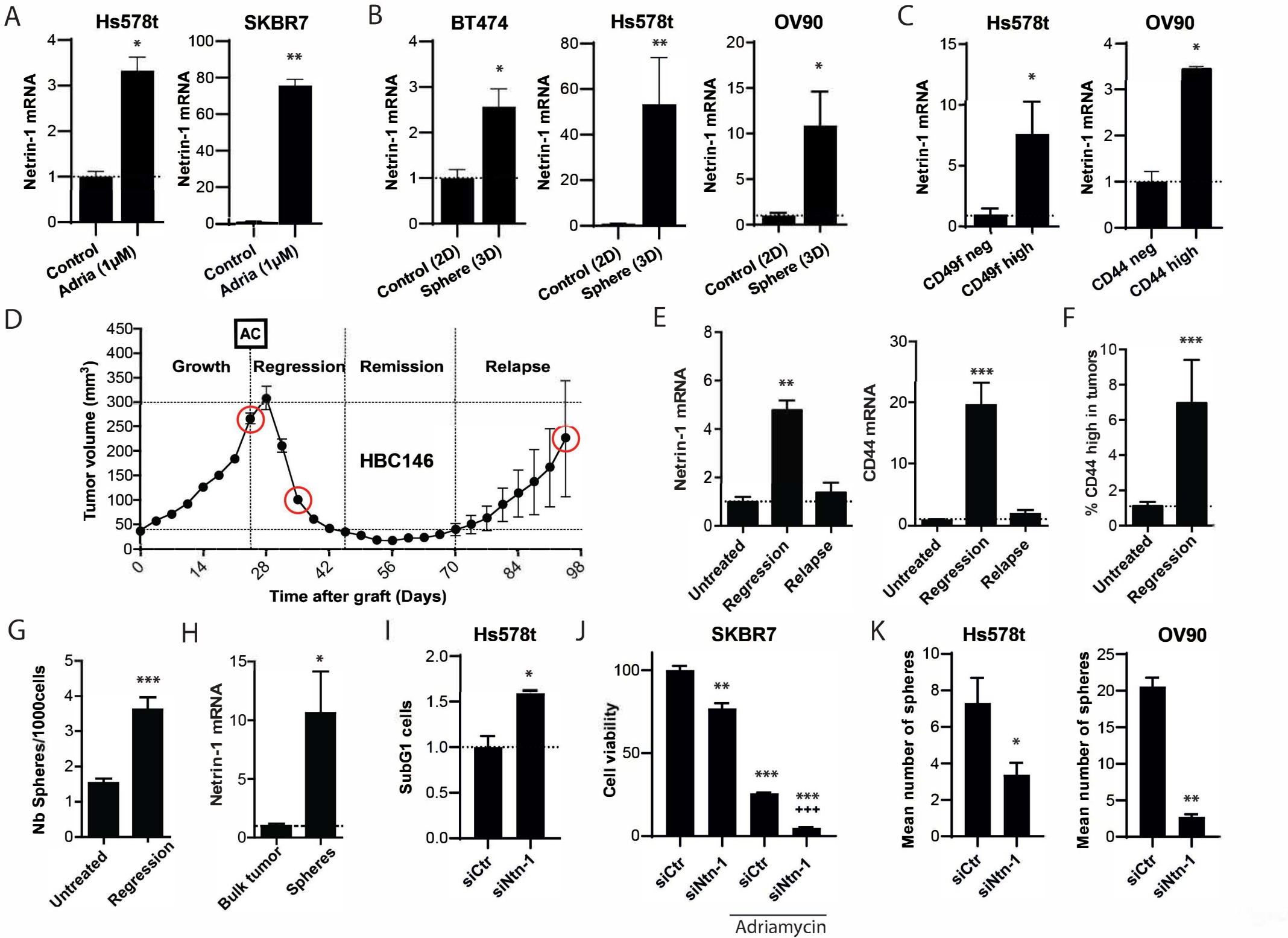
A
Hs578t
SKBR7
Netrin-1 mRNA
Control
Adria (1µM)
B
BT474
Hs578t
OV90
Control (2D)
Sphere (3D)
C
Hs578t
OV90
CD49f neg
CD49f high
CD44 neg
CD44 high
D
AC
Growth
Regression
Remission
Relapse
HBC146
Tumor volume (mm3)
Time after graft (Days)
E
Netrin-1 mRNA
CD44 mRNA
Untreated
Regression
Relapse
F
% CD44 high in tumors
G
Nb Spheres/1000cells
H
Bulk tumor
Spheres
I
SubG1 cells
siCtr
siNtn-1
J
SKBR7
Cell viability
Adriamycin
K
Mean number of spheres

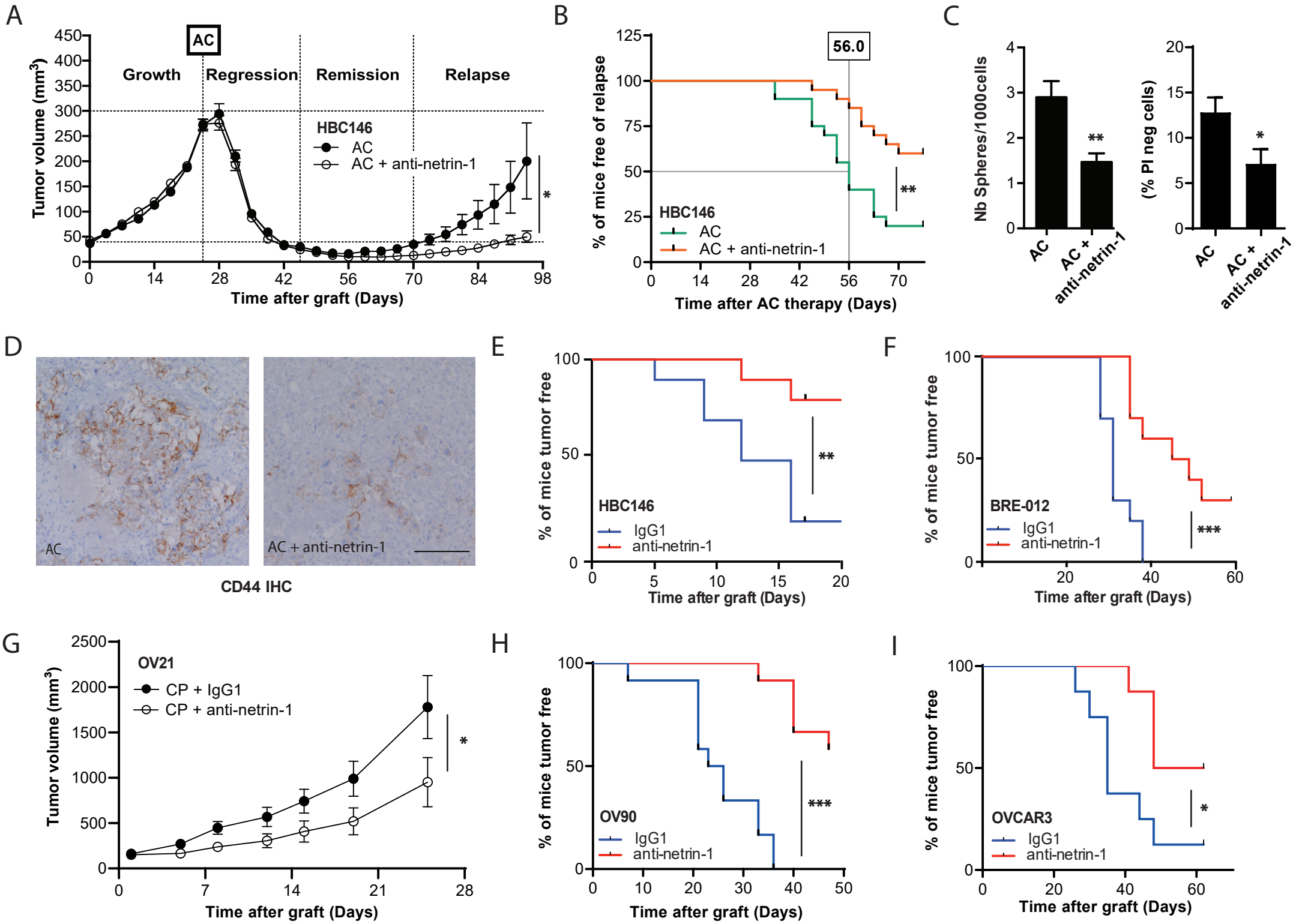
A
AC
Growth
Regression
Remission
Relapse
Tumor volume (mm3)
HBC146
AC
AC + anti-netrin-1
*
Time after graft (Days)
B
56.0
% of mice free of relapse
HBC146
AC
AC + anti-netrin-1
**
Time after AC therapy (Days)
C
Nb Spheres/1000cells
**
AC
AC + anti-netrin-1
(% PI neg cells)
*
AC
AC + anti-netrin-1
D
AC
AC + anti-netrin-1
CD44 IHC
E
% of mice tumor free
HBC146
IgG1
anti-netrin-1
**
Time after graft (Days)
F
% of mice tumor free
BRE-012
IgG1
anti-netrin-1
***
Time after graft (Days)
G
Tumor volume (mm3)
OV21
CP + IgG1
CP + anti-netrin-1
*
Time after graft (Days)
H
% of mice tumor free
OV90
IgG1
anti-netrin-1
***
Time after graft (Days)
I
% of mice tumor free
OVCAR3
IgG1
anti-netrin-1
*
Time after graft (Days)

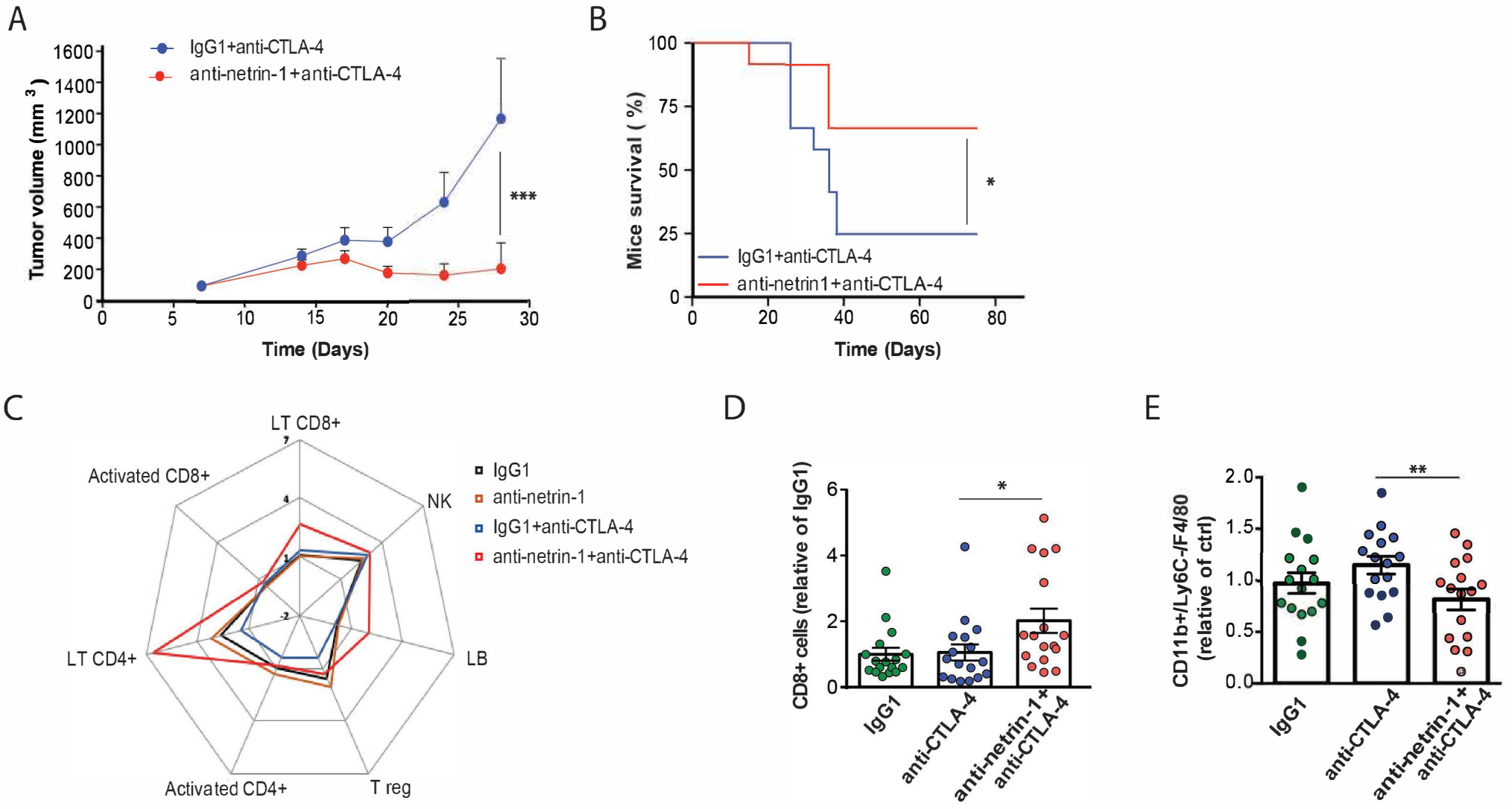
A
IgG1+anti-CTLA-4
anti-netrin-1+anti-CTLA-4
Tumor volume (mm 3)
1600
1400
1200
1000
800
600
400
200
0
0
5
10
15
20
25
30
Time (Days)
***
B
100
75
50
25
0
Mice survival (%)
IgG1+anti-CTLA-4
anti-netrin1+anti-CTLA-4
0
20
40
60
80
Time (Days)
*
C
LT CD8+
Activated CD8+
NK
LT CD4+
LB
Activated CD4+
T reg
IgG1
anti-netrin-1
IgG1+anti-CTLA-4
anti-netrin-1+anti-CTLA-4
D
CD8+ cells (relative of IgG1)
6
4
2
0
*
IgG1
anti-CTLA-4
anti-netrin-1+
anti-CTLA-4
E
CD11b+/Ly6C-/F4/80
(relative of ctrl)
2.0
1.5
1.0
0.5
0.0
**
IgG1
anti-CTLA-4
anti-netrin-1+
anti-CTLA-4

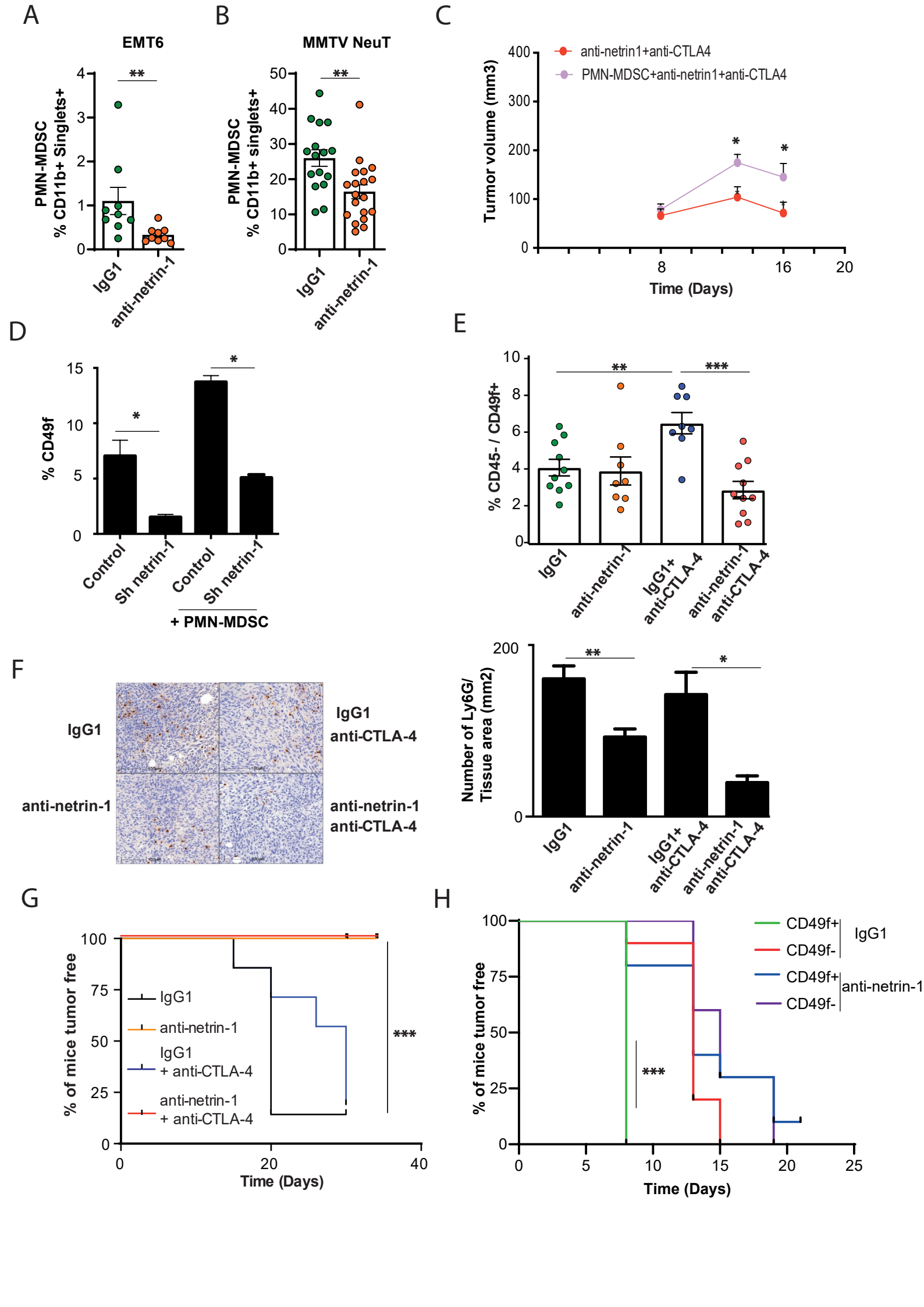
A
EMT6
PMN-MDSC
% CD11b+ Singlets+
IgG1
anti-netrin-1
B
MMTV NeuT
PMN-MDSC
% CD11b+ singlets+
IgG1
anti-netrin-1
C
anti-netrin1+anti-CTLA4
PMN-MDSC+anti-netrin1+anti-CTLA4
Turmor volume (mm3)
Time (Days)
D
% CD49f
Control
Sh netrin-1
Control
Sh netrin-1
+ PMN-MDSC
E
% CD45- / CD49f+
IgG1
anti-netrin-1
IgG1+ anti-CTLA-4
anti-netrin-1 anti-CTLA-4
F
IgG1
IgG1 anti-CTLA-4
anti-netrin-1
anti-netrin-1 anti-CTLA-4
Number of Ly6G/ Tissue area (mm2)
IgG1
anti-netrin-1
IgG1+ anti-CTLA-4
anti-netrin-1 anti-CTLA-4
G
% of mice tumor free
IgG1
anti-netrin-1
IgG1 + anti-CTLA-4
anti-netrin-1 + anti-CTLA-4
Time (Days)
H
% of mice tumor free
CD49f+
CD49f-
IgG1
CD49f+
CD49f-
anti-netrin-1
Time (Days)

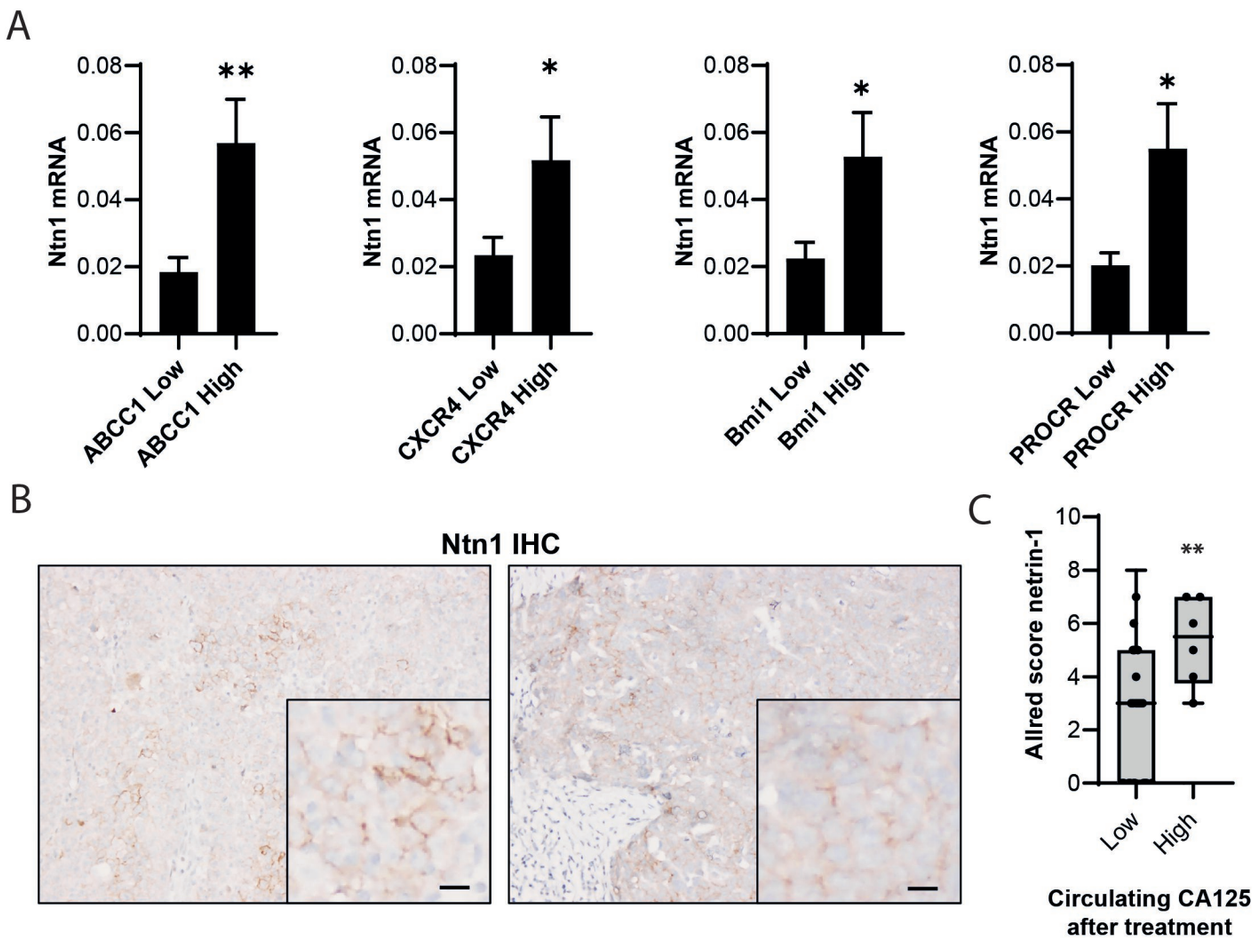

Supplementary Figure 1

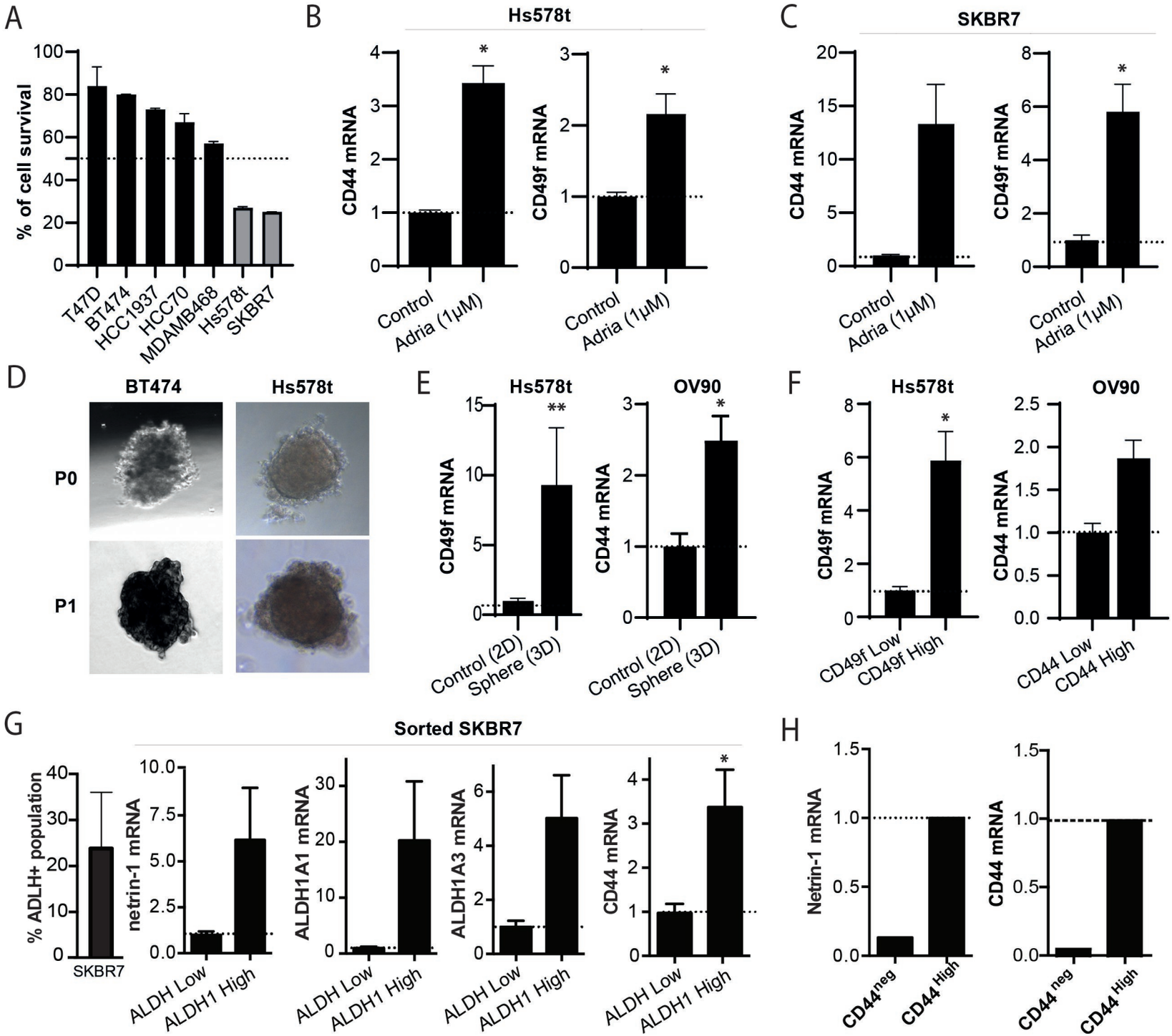

Supplementary Figure 2

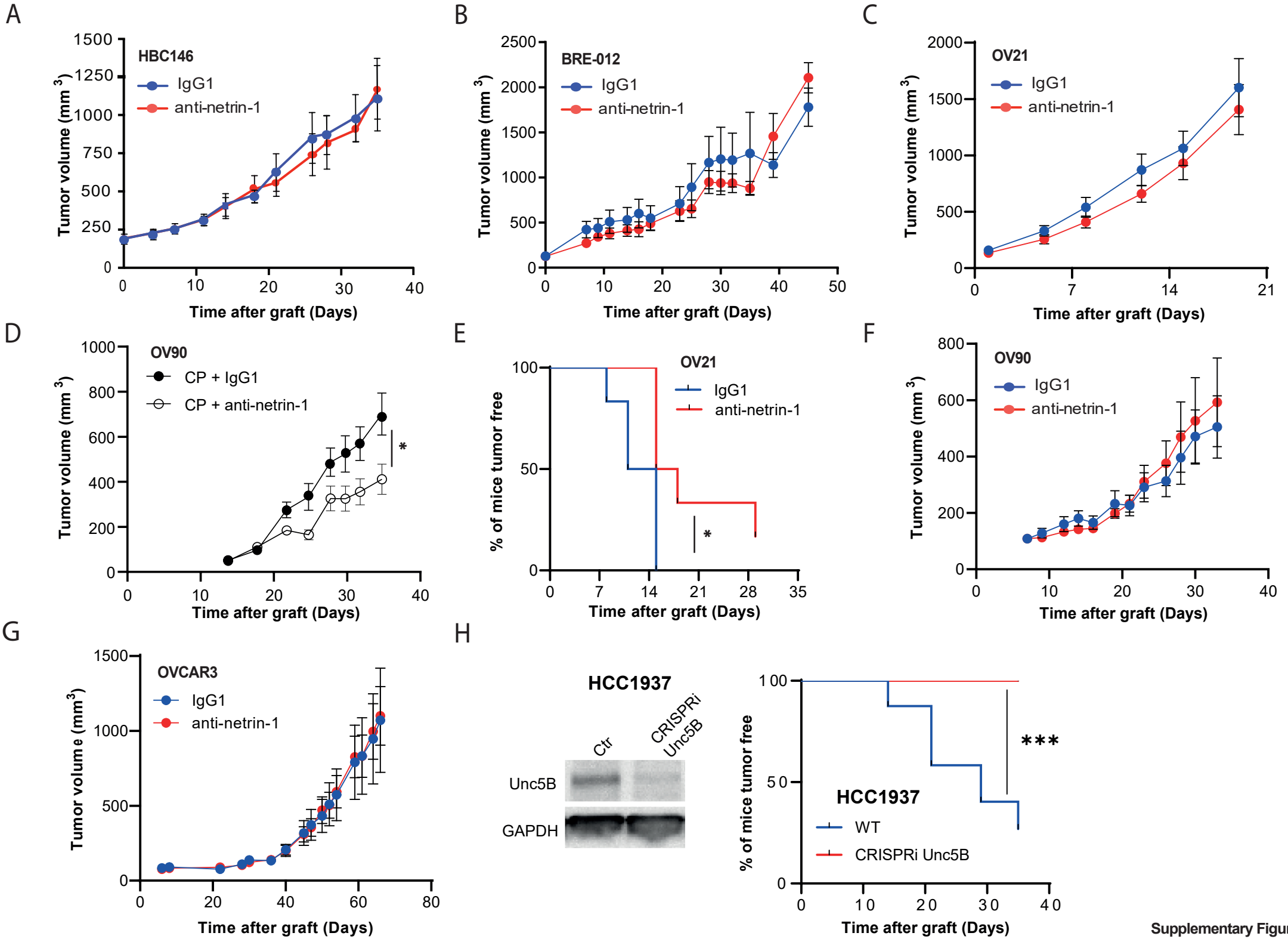

Supplementary Figure 3

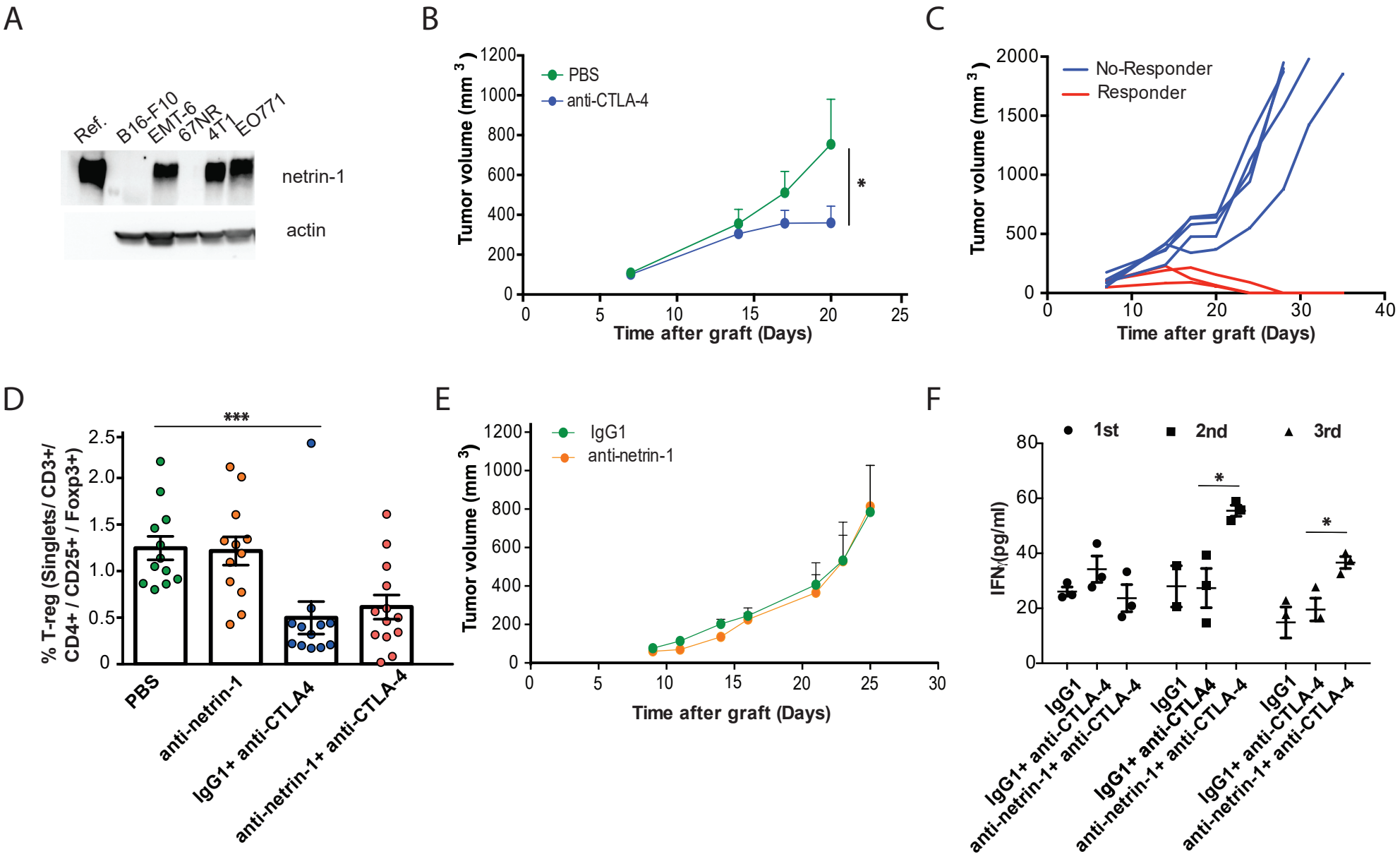

Supplementary Figure 4

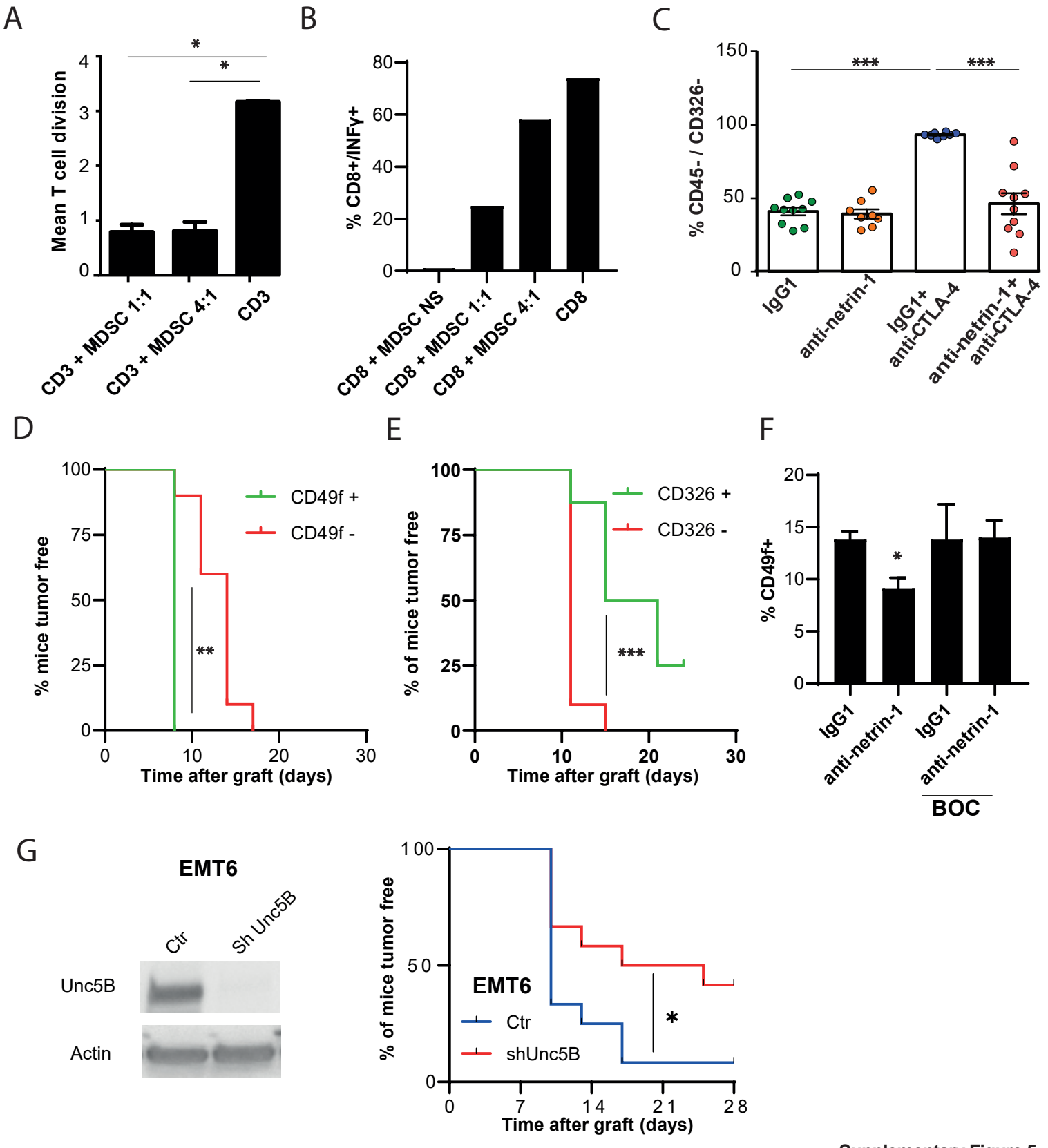

Supplementary Figure 5